Cell Reports

Article

Optogenetic Stimulation of Basal Forebrain Parvalbumin Neurons Activates the Default Mode Network and Associated Behaviors

Graphical Abstract

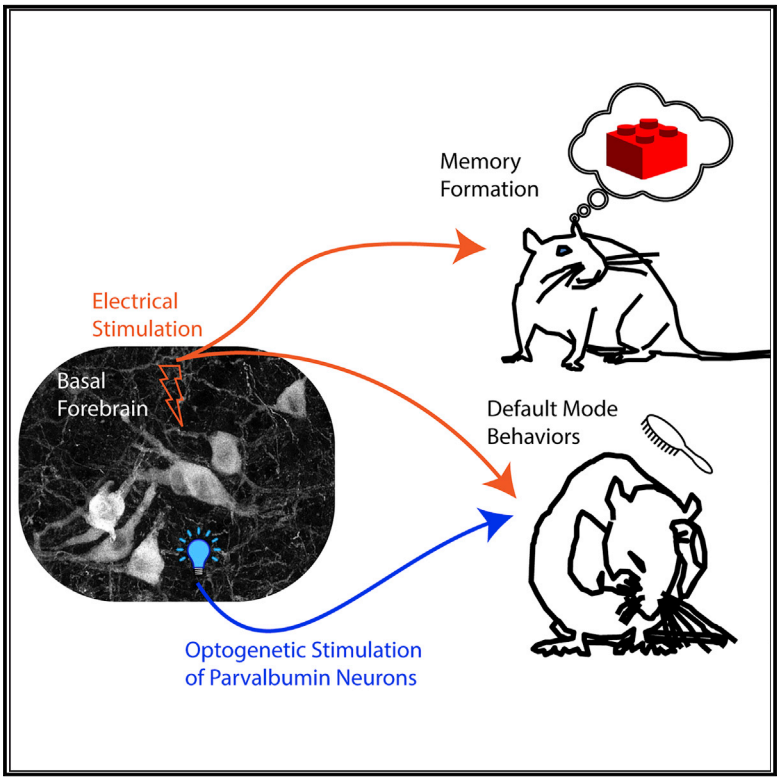

Authors

Laura Lozano-Montes, Marta Dimanico, Reza Mazloum, ...,
Ralf Schneggenburger, Michael Harvey, Gregor Rainer

Correspondence

gregor.rainer@unifr.ch

In Brief

The default mode network (DMN) is a group of brain areas activated during inwardly focused attention. Lozano-Montes et al. show that optogenetically activating basal forebrain (BF) PV^+ neurons initiate behaviors associated with the DMN, validating BF as a DMN node and implicating BF PV^+ neurons as regulators of DMN activity.

Highlights

- Activation of PV^+ neurons in basal forebrain (BF) drives animals to self-directed behaviors
- BF electrical stimulation affects memory formation and behavior
- BF stimulation affects behaviors associated with the default mode network (DMN)
- BF electrical stimulation drives correlated changes in neuropeptides in DMN nodes

Lozano-Montes et al., 2020, Cell Reports *33*, 108359
November 10, 2020
https://doi.org/10.1016/j.celrep.2020.108359

CellPress

Cell Reports

CellPress
OPEN ACCESS

Article

Optogenetic Stimulation of Basal Forebrain Parvalbumin Neurons Activates the Default Mode Network and Associated Behaviors

Laura Lozano-Montes,[1] Marta Dimanico,[1] Reza Mazloum,[1] Wenxue Li,[1] Jayakrishnan Nair,[1] Michael Kintscher,[2] Ralf Schneggenburger,[2] Michael Harvey,[1] and Gregor Rainer[1,3,*]

[1]Section of Medicine, University of Fribourg, 1700 Fribourg, Switzerland

[2]Laboratory of Synaptic Mechanisms, Brain Mind Institute, School of Life Science, École Polytechnique Fédérale de Lausanne (EPFL), 1015 Lausanne, Switzerland

[3]Lead Contact

*Correspondence: gregor.rainer@unifr.ch

https://doi.org/10.1016/j.celrep.2020.108359

SUMMARY

Activation of the basal forebrain (BF) has been associated with increased attention, arousal, and a heightened cortical representation of the external world. In addition, BF has been implicated in the regulation of the default mode network (DMN) and associated behaviors. Here, we provide causal evidence for a role of BF in DMN regulation, highlighting a prominent role of parvalbumin (PV) GABAergic neurons. The optogenetic activation of BF PV neurons reliably drives animals toward DMN-like behaviors, with no effect on memory encoding. In contrast, BF electrical stimulation enhances memory performance and increases DMN-like behaviors. BF stimulation has a correlated impact on peptide regulation in the BF and ACC, enhancing peptides linked to grooming behavior and memory functions, supporting a crucial role of the BF in DMN regulation. We suggest that in addition to enhancing attentional functions, the BF harbors a network encompassing PV GABAergic neurons that promotes self-directed behaviors associated with the DMN.

INTRODUCTION

The basal forebrain (BF) has long been known to contribute to attention—that is; the allocation of brain resources to the encoding of incoming sensory stimuli (Baxter and Chiba, 1999; Dotigny et al., 2008; Harris and Thiele, 2011; Herrero et al., 2008; Kang and Vaucher, 2009; Quinn et al., 2010; Xu et al., 2015; Zaborszky and Duque, 2003; Zaborszky et al., 1999; Zinke et al., 2006). For example, neurons in primary visual cortex (VC; V1) become more responsive to visual stimuli following BF activation (Alitto and Usrey, 2003; Bhattacharyya et al., 2012, 2013; Soma et al., 2011), demonstrating an upregulation of the cortical stimulus representation. Along related lines, both single-unit and local field potential responses in V1 exhibit increased trial-to-trial reliability (De Luna et al., 2017; Goard and Dan, 2009; Pinto et al., 2013), facilitating decision making on the basis of sensory evidence. Many of these effects have been directly linked to the cholinergic BF corticopetal projection system, which is consistent with the observation that the BF is the major source of cortical acetylcholine (Laplante et al., 2005; Mesulam et al., 1983). Accordingly, augmenting cholinergic release in the cortex improves visual learning, enhances visual evoked cortical potentials, and upregulates the density of cholinergic receptors (Chamoun et al., 2016; Kang et al., 2014; Sato et al., 1987; Wonnacott, 1990). Available evidence thus suggests that the activation of BF cholinergic projections triggers a cortical state of elevated vigilance and attention to sensory stimuli, consistent with favoring subcortical over cortico-cortical inputs (Hsieh et al., 2000).

Recently, we have described very pronounced gamma oscillations in the BF (Nair et al., 2016), during quiet wakefulness that were suppressed when animals engaged in active exploration of the environment (Nair et al., 2018). While gamma oscillations are a multifaceted phenomenon whose functional role is at present debated (Ray and Maunsell, 2015; Buzsáki and Wang, 2012; Lachaux et al., 2005; Kirschfeld, 1992), it appears clear that they generally occur in conjunction with elevated local spiking activity and are related to local excitation of neural circuits. The suppression of gamma oscillations during exploration is thus highly unexpected based on the previous literature related to cholinergic BF modulation, because the attention-demanding exploration phase is associated with low BF gamma activity, whereas during the task-off period, gamma oscillations are highly prominent. The BF gamma activity profile resembles that of the cortical default mode network (DMN), a collection of cortical areas, including the anterior cingulate (ACC) and retrosplenial cortices (RSCs), that is active during quiet wakefulness and internally focused processing in humans (Raichle et al., 2001; Greicius et al., 2003; Raichle, 2015). It is becoming increasingly clear that rodents, particularly rats, also have a DMN, which includes brain regions homologous to those observed in humans. For example, several studies have shown functional connectivity between rat ACC and other midline structures including RSCs (Hsu et al., 2016;

Lu et al., 2012). Using fMRI in awake restrained rats, Upadhyay et al. (2011) have demonstrated an ACC-RSC-hippocampal functional connectivity. Interestingly, this functional connectivity only developed over testing days as the animals became adapted to the testing situation. This supports the idea that with prolonged exposure to the scanner environment, animals attained a state of quiet wakefulness with concomitant activation of the DMN. Early in testing, ACC and RSC in fact exhibited an inverse functional relationship, with ACC being functionally coupled with what the authors call an anxiety network, including the hypothalamus and amygdala. Over testing days, as the animals become habituated to the test situation, their respiratory rate and head movements decrease, and ACC becomes positively coupled with traditional DMN areas, including the RSCs and hippocampus. As in humans, activity in the medial structures, including the ACC and RSCs, is anti-correlated with activity in the lateral secondary sensorimotor system (Schwarz et al., 2013). Finally, ACC involvement in a rodent DMN has also been shown, both structurally and functionally in mice using fMRI and axonal tracing (Stafford et al., 2014), suggesting that a functional DMN that includes ACC is a general property of the rodent brain. Based on correlative evidence, we therefore hypothesized that the BF may indeed be a subcortical node of the DMN; a notion that is supported by functional imaging studies in macaques and humans (Alves et al., 2018, 2019; Turchi and Sarter, 1997). The BF parvalbumin positive (PV^+) GABAergic corticopetal projection neurons are the most likely candidates for the anatomical substrate of BF participation in DMN regulation. This population projects specifically to anterior cingulate and retrosplenial cortices, two major DMN nodes (Do et al., 2016) and GABAergic PV neurons have been linked to cortical gamma oscillations (Cardin et al., 2009; Kim et al., 2015; Kimura et al., 1999). In the present study, we set out to examine the effects of optogenetic activation of the BF PV projection neurons on the brain and behavioral state, with a particular view to test the hypothesis of a functional role of the BF PV population in DMN state regulation.

RESULTS

To study the specific effects of BF PV neuron activations on exploratory behaviors, recognition memory, and default mode behavioral and brain states, we used a transgenic PV:Cre rat. We tested the specificity and potency of this transgenic model for optogenetic experiments (Figure 1). We studied the expression of two different Cre-dependent viral constructs, adeno-associated virus type 5 (AAV5)-ChR2-mCherry and AAV8-Chronos-GFP, both of which resulted in highly specific opsin expression in PV neurons (Figures 1A–1C). We anticipated that among BF nuclei, the magnocellular preoptic nucleus (MCPO) would show a high density of PV neurons (McKenna et al., 2013), and this was in fact the case (see Figure 1B, PV expression). We determined the co-expression of PV and viral constructs by manual cell counting in MCPO (see Figure 1C for a typical example of co-expression analysis). For the AAV5-ChR2 injections, we counted 1,133 neurons showing either Cre-dependent fluorophore (mCherry) expression or immunohistochemical labeling for PV (Alexa 488 fluorophore). For AAV5-ChR2-mCherry, we observed a potency of 52% ± 2.5% corresponding to the number of PV^+ cells expressing ChR2 and a specificity of 93.5% ± 1.0%, corresponding to the number of ChR2-expressing cells that were PV^+. We found similar values for AAV8-Chronos-eGFP (n = 707), with a potency of 45.4% ± 4.4% and a specificity of 95.2% ± 0.2% (Figure 1D, right). Specificity and potency values were thus highly similar for the two viral constructs, and values in the present study were within the range of previously reported Cre-dependent models (Kalenscher et al., 2010; Oh et al., 2017; Witten et al., 2011).

For functional *in vitro* validation, we performed whole-cell patch recordings of MCPO neurons in a slice preparation (see Method Details). As illustrated by the example neurons in Figure 1E, brief blue light pulses depolarized the membrane potential and triggered action potentials in patched cells expressing AAV8-Chronos-GFP^+ (right panels), while having no impact on control (GFP^-) neurons (left panel). As expected, light intensity was positively correlated with the magnitude of the depolarization, as well as with spiking probability (n = 10; Figure 1F). We note that a light irradiance >2 mW/mm^2 was sufficient to elicit robust spiking in GFP^+ neurons. We estimated the frequency response of optogenetically induced spiking to pulse trains of blue light stimulation at five frequencies. We observed that light pulses reliably triggered action potentials over a range of frequencies up to ~50 Hz, while spiking probability decreased at higher frequencies of stimulation (Figure 1G). These results provide *in vitro* validation for the PV:Cre rat model system for optogenetic studies and suggest that light stimulation protocols with laser intensities of at least 2 mW/mm^2 and stimulation frequencies up to ~50 Hz appear to be optimal.

For functional *in vivo* validation, we implanted rats with optrodes targeting the MCPO following viral injections and recorded local field potentials (LFPs) during optogenetic pulse stimulation at various frequencies while animals were not engaged in any particular task. We found that *in vivo* optical activations at different frequencies (20, 30, 40, 50, and 60 Hz, 10-ms pulses) elicited narrow-band LFP responses at the stimulation frequency, and in some cases, also at the corresponding harmonics. Example recordings from a representative rat (AAV5-ChR2) are shown in Figure 2A, highlighting that BF PV stimulation up to 60 Hz reliably activates BF circuits *in vivo*. We analyzed the changes in LFP spectral power between baseline and the optically activated epochs at different stimulation frequencies. Significant spectral peaks that fall within the gamma range for an example recording are summarized in Figure 2B. We found that the 30-Hz stimulation protocol was the only protocol that reliably generated 2 spectral peaks within the endogenous gamma range (~30–80 Hz; i.e., peaks at both the fundamental [30 Hz] and 2^{nd} harmonic [60 Hz] frequencies). Since the endogenous gamma range is of particular interest in the context of the BF and its relation the DMN (Nair et al., 2016, 2018), we selected the 30-Hz stimulation frequency for use in our behavioral studies. To validate the 30-Hz stimulation protocol for Chronos and ChR2, we optically stimulated groups of animals participating in later behavioral experiments. LFP spectral analysis of two example animals confirmed the presence of both the 30- and 60-Hz peaks (Figure 2C). We observed enhanced 30- and 60-Hz peaks at most of our BF recording sites (n = 13) taken from 3 ChR2 and 4 Chronos injected animals (Figure 2D). An unpaired t test with Welch's correction showed no difference in the

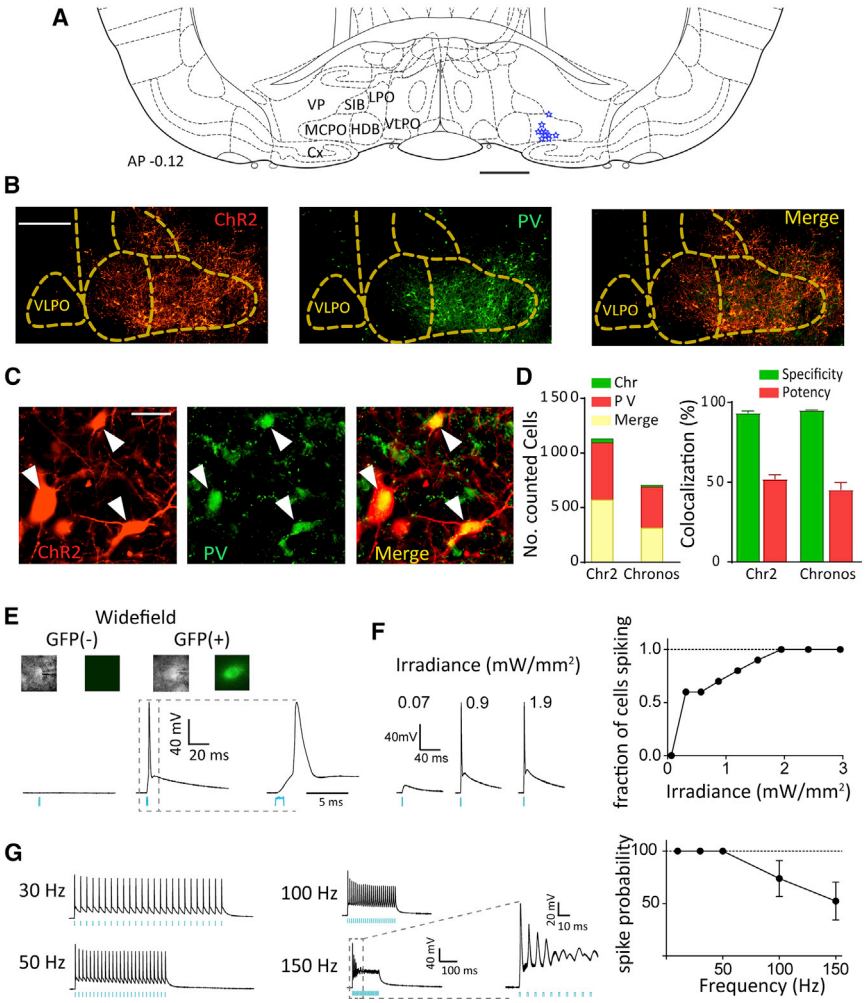

Figure 1. Opsin Expression and Functional Validation of PV:Cre Rats

(A) Schematic showing optical stimulation sites (blue stars) within the MCPO region from 10 animals included in our study; section taken 0.12 mm posterior to bregma.

(B) Example of PV immunofluorescence and Chr2 m-Cherry expression at the injection site.

(C) Co-localization of PV and ChR2-mCherry expression in MCPO cell bodies.

(D) The number of counted cells that were positive for PV, channel protein (Chr2 or Chronos), or both (merge) is shown on the left. The percentage of cells that were positive for Chr2 or Chronos that were also PV^+ (specificity) and the percentage of all PV^+ cells that were transfected (potency) are shown at right. Cx, cerebral cortex; HDB, horizontal limb diagonal band; LPO, lateral preoptic area; MCPO, magnocellular preoptic nucleus; SIB, substantia innominata; VLPO, ventrolateral preoptic nucleus; VP, ventral pallidum.

(E) Example current-clamp recording of a PV^- neuron (left) and a PV^+ neuron (right). The top panel shows the patched cell in wide field and fluorescence microscopy. Voltage traces are shown in black and the detection of 1-ms light (480 nm) pulses by the photodiode in blue.

(F) Spike probability versus irradiance for PV^+ neurons. Representative voltage traces for 1-ms light pulse and increasing irradiance (left panel). Summary data for the fraction of cells spiking at the respective irradiance (n = 10; right panel).

(G) Spike fidelity versus frequency for 25 × 1-ms light pulses. Representative Chronos-expressing PV:Cre neurons are able to reliably follow light-evoked pulse trains over a range of frequencies (left panel). Summary data for spike probability (% of successful spikes, means ± SEMs) to different frequencies of optical activations in Chronos-expressing PV:Cre neurons (n = 5; right panel); n = technical replicates.

Scale bars: (A) 1 mm; (B) 0.5 mm; (C) 50 μm.

average percentage increase between Chronos and ChR2 animals (30 Hz peak: t(3.217) = 0.7664, p = 0.4958; 60 Hz: t(3.46) = 1.145, p = 0.3253). We were also interested in how our BF PV stimulation would affect cortical areas known to be part of the DMN. Since we have previously shown that endogenous BF gamma activity is related to gamma oscillations in the ACC (Nair et al., 2018), we recorded ACC activity during BF PV optical stimulation. In 3 of 5 animals with ACC electrodes, the ACC was highly entrained by 30 Hz BF PV stimulation evidenced by significant (paired t test; $p < 0.001$) increases in fast Fourier transform (FFT) power at the stimulation frequency (see Figure 2E for a representative example). Optical activation did not elicit any LFP spectral peaks in control animals injected with empty virus (data not shown). These results indicate that the 30-Hz PV neuron stimulation protocol robustly activated BF neural circuits, as well as other nodes of the DMN, and elicited similar BF gamma band LFP enhancement in both the Chronos and ChR2 animals.

Next, we characterized the impact of optical activation of the BF PV neural circuits on rat behavior. According to our hypothesis, these PV circuits may bias animals toward behaviors associated with DMN activation and the associated default brain state. Therefore, animals should be less disposed to engage in exploratory and foraging behaviors following BF PV stimulation. To test this hypothesis in an initial behavioral experiment, we used a surface food test. Here, rats were presented with a readily visible, familiar, palatable food item in a test chamber (see Method Details; Figure 2F). PV (Chronos-AAV8, N = 3) activation during the 10 min before food item presentation increased the latency of the animals to retrieve the item relative to empty virus injected control animals undergoing identical optical stimulation (AAV8, N = 4), (t(5) = 8.792, p = 0.0003; Figure 2F). No differences were observed in the time spent eating the food item between these groups (t(5) = 0.5086, p = 0.6327), suggesting that the regulation of food intake was not affected by BF PV activation. This is consistent with a previous study in the BF, ascribing an important role to BF somatostatin (SST) neurons, but not BF PV neurons in the regulation of feeding and associated motivational processing (Zhu et al., 2017). We interpret our findings as resulting from reduced exploratory drive due to BF PV concomitant DMN activation.

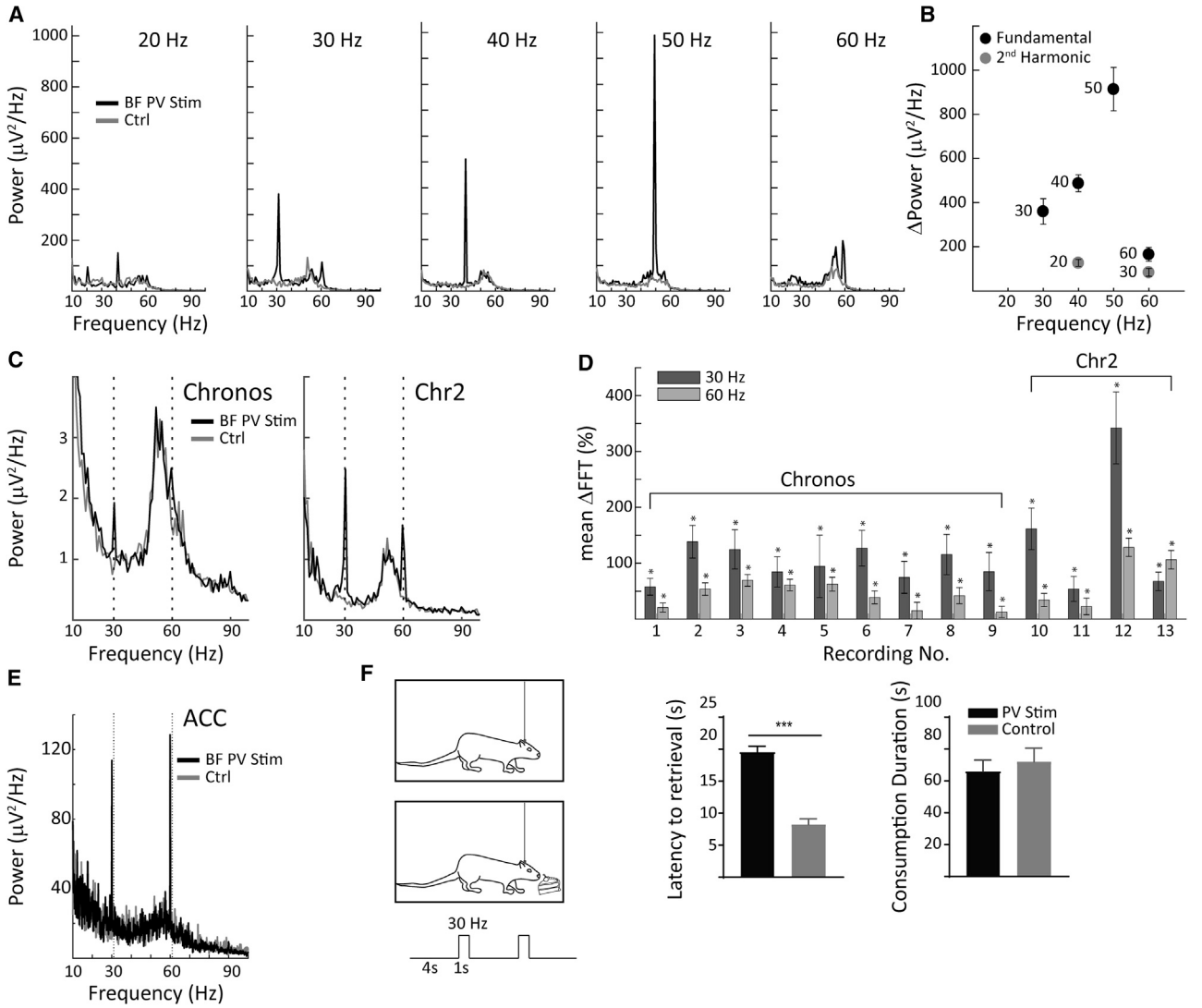

Figure 2. Spectral Properties of BF LFP Responses to Optical Stimulation and Exploratory Behavior

(A) Representative examples from a single animal showing that LFPs in the BF are locked to the optical stimulation frequency between 20 and 60 Hz, and occasionally its harmonics.

(B) Significant increases within the gamma range in the FFT of LFP recordings at the fundamental and the 2nd harmonic of all stimulation frequencies (text adjacent to the symbols) are plotted. As only 30 Hz stimulation resulted in 2 significant peaks within the gamma range (30–80 Hz), we chose this frequency for subsequent tests.

(C) Individual examples for both a Chronos and Chr2 animal showing equivalent spectral response properties in the LFP during 30-Hz BF PV activation.

(D) 30-Hz BF PV stimulation resulted in significant increases at both the fundamental and 2nd harmonic (30 and 60 Hz) at 13 BF recording sites from 7 animals, independent of the channel protein used (Chronos 1–9 and Chr2 10–13).

(E) Representative example of power spectra from LFP recordings in the ACC during control and 30 Hz BF PV stimulation. In 3 of 5 animals with ACC electrodes, 30-Hz BF PV stimulation gave rise to significant FFT peaks at 30 and 60 Hz.

(F) Schematic of the surface food test followed by BF PV-stimulated (N = 3) and control (N = 4) animals (left panel); N = biological replicates. Stimulated animals showed higher latencies to food retrieval than control animals; however, no differences were found in the duration of food consumption between the 2 groups, right panel. Error bars reflect +/− SEM.

Given this evidence, we decided to examine in more detail the effects of BF PV stimulation on explorative behaviors in the novel object recognition (NOR) test, a widely used paradigm (Antunes and Biala, 2012; Mathiasen and Dicamillo, 2010) for testing exploration and memory encoding in laboratory animals. After eight sessions of habituation to an arena, rats completed four sessions of object training during which two identical objects were presented (Figure 3A). On the last training session, T4, PV BF neurons were stimulated optically at 30 Hz while rats performed the task. The following day (session TEST), a novel object was introduced into the arena, replacing one of the familiar objects. We validated the NOR test for both PV-stimulated

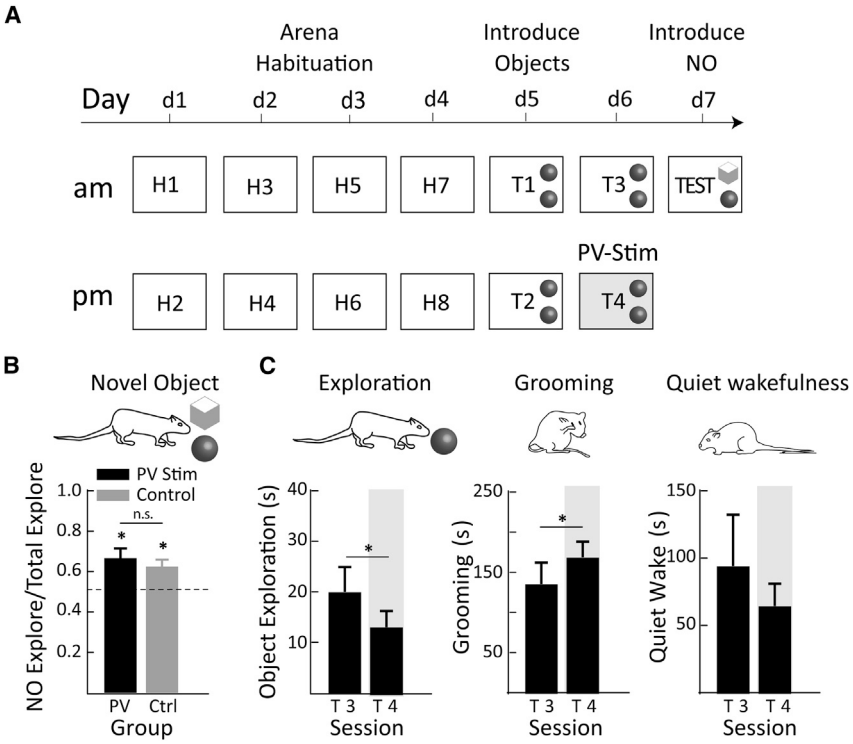

Figure 3. Effects of BF PV Stimulation on Novel Object Recognition (NOR) and DMN Behaviors in PV:Cre Rats

(A) Schematic of the NOR test followed by BF PV-stimulated (n = 8) and control (n = 7) animals. Optical stimulation took place on the last session of training phase T4 (gray shading).

(B) Performance on the NOR in BF PV-stimulated and control groups is defined as the ratio of time spent exploring the novel object over total object exploration time (i.e., including the familiar object). Using this measure, both groups spent significantly more time exploring the NO than the familiar object; however, no significant difference between novelty preference ratios for stimulated and control animals was found.

(C) Within-animal comparisons were performed to study differences on exploratory and DMN-like behaviors of BF PV-stimulated animals (n = 8) between the T3 and T4 (optical activation session; right panel). Stimulated animals significantly decreased the average duration of exploration of familiar objects and grooming duration was significantly increased; however, there were no significant changes in quiet wakefulness duration between T3 and T4 session. Error bars reflect +/− SEM.

(ChR2-AAV5, N = 3; Chronos-AAV8, N = 5) and empty virus-injected (AAV5, N = 3; AAV8, N = 4) control animals undergoing identical optical stimulation, by demonstrating that both groups exhibited a preference for the novel object on the day after BF PV stimulation. Accordingly, novelty preference ratios (Gaskin et al., 2010) of PV-stimulated animals and empty virus controls exceeded a value of 0.5 ($t(7) = 3.189$, $p = 0.0153$; $t(6) = 3.714$, $p = 0.0099$, respectively). We found no significant difference between novelty preference ratios of PV-stimulated and control animals ($t(13) = 0.6533$, $p = 0.5249$; Figure 3B). Because preference for the novel object necessitates intact memory for the familiar object, the NOR test results suggest that BF PV stimulation did not have a significant impact on memory formation. It is important to examine whether opsin expression in these animals induced any notable behavioral abnormalities even in the absence of optical stimulation. Accordingly, we performed rater-blind video scoring of the initial object training session (T1) for the behaviors of object exploration, self-grooming, and quiet wakefulness. We found no differences in terms of these behaviors between the 2 groups of animals (unpaired t tests examining duration of object exploration, self-grooming and quiet wakefulness ($t(13) = 0.1994$, $p = 0.8451$; $t(13) = 0.7518$, $p = 0.4656$; $t(13) = 1.067$, $p = 0.3056$, respectively). We conclude that opsin expression in PV-Cre rats does not produce any overt behavioral abnormalities in terms of the parameters quantitatively assessed here.

While BF PV stimulation had no effect on memory formation (i.e., no effects on novelty preference on the subsequent day), it may nevertheless affect rat behavior during optical stimulation in the object training session. To assess whether this was the case, we compared the duration of behaviors of interest between object training sessions T3 and T4 for stimulated and control rats, a strategy that takes into consideration inter-individual differences among animals, and thus provides a sensitive test of potential behavioral effects. The findings are summarized in Figure 3C. We observed a significant decrease in average object exploration during PV stimulation ($t(7) = 2.785$, $p = 0.0271$), while no significant changes were observed in the control group ($t(6) = 0.948$, $p = 0.3797$). BF PV activation thus slightly decreased object exploration in the NOR task, similar to the results of the visible food test documented above, with both findings being consistent with BF PV activation's triggering the default brain state. Given that PV stimulation decreased the exploratory behaviors of the animals, we then tested whether the DMN-like behaviors would be enhanced during PV activation. Self-grooming and quiet wakefulness are behaviors in which the animals are not exploring the surrounding environment and are involved in self-directed behaviors, compatible with DMN activation, as previously described (Nair et al., 2018). A paired t test showed an increase in self-grooming between the T3 and T4 sessions for the PV-stimulated but not the control animals ($t(7) = 2.843$, $p = 0.0249$; $t(6) = 0.3116$, $p = 0.7659$), while no differences were observed in the amount of time spent in quiet wakefulness ($t(7) = 1.328$, $p = 0.2260$; $t(6) = 1.015$, $p = 0.3493$). These results suggest that the 30-Hz optical activation of BF PV neurons enhances one aspect of default brain state-associated behavior (i.e., self-grooming), while not affecting quiet wakefulness.

To gain further insight into the impact of optogenetic PV neuron activation on neural circuit activity and its relation to behavior, we studied BF LFPs in object training session T4.

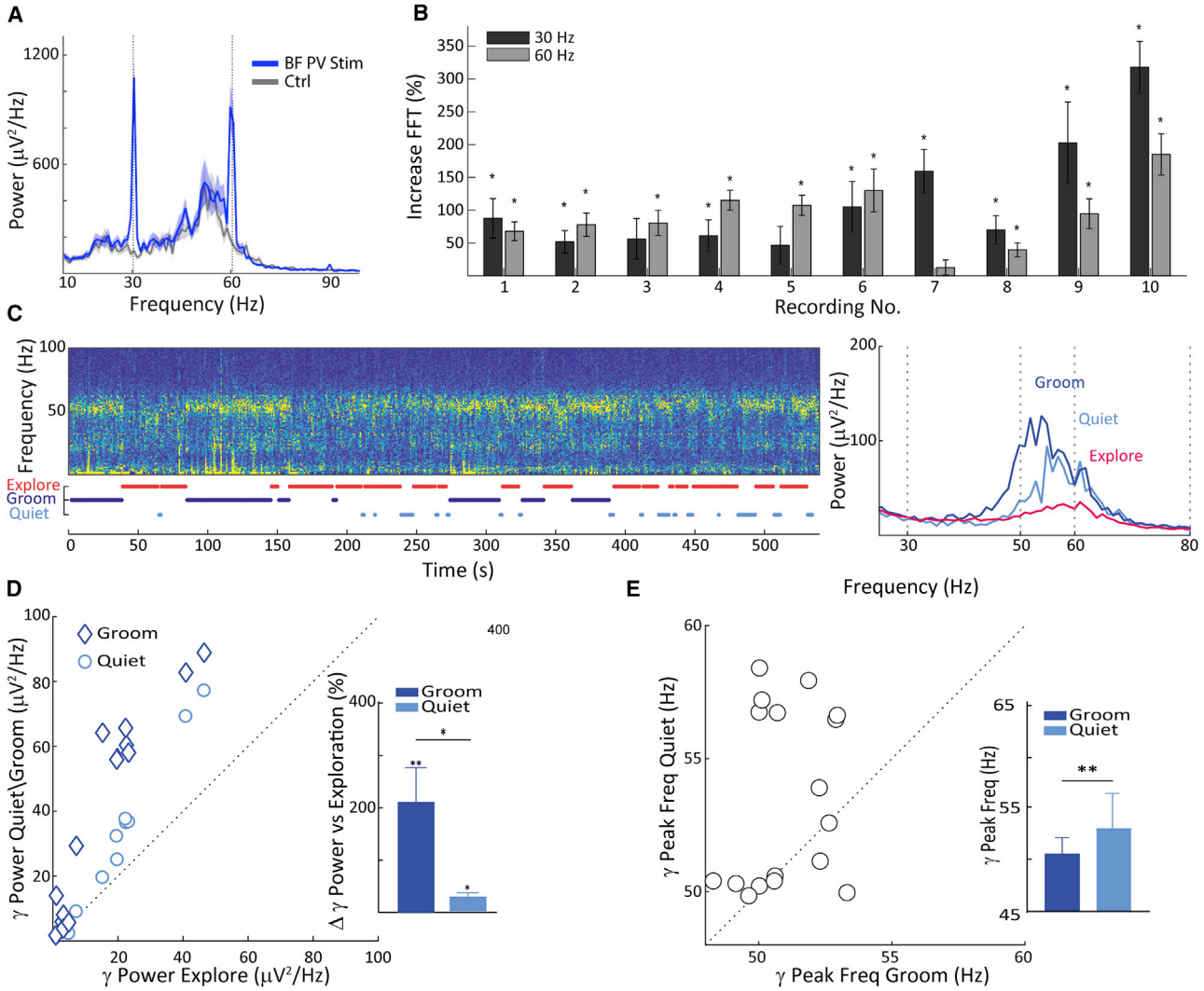

Figure 4. BF Gamma Power and DMN-like Behaviors

(A) Average LFP power during 30-Hz optical stimulation (blue) and control epochs (gray) during the NOR test.

(B) Percentage increase in the ΔFFT power over control epochs at 30 and 60 Hz for 10 BF recording sites. Error bars reflect +/− SEM.

(C) Single-session LFP spectrogram of BF activity in the NOR arena. During this period, behavior was scored for exploration (red), grooming (blue), and quiet wakefulness (cyan), shown below the spectrogram. The average BF gamma power during these 3 behaviors are shown to the right, where the behavioral state is associated with changes in both peak power and amplitude.

(D) Broadband gamma power (30–80 Hz) during arena exploration is plotted against gamma power during both grooming and quiet wakefulness, showing, as for the individual example in (C), that gamma power is higher during DMN-like behaviors for the population as a whole.

(E) Also as exemplified in (C), gamma peak frequency was higher during quiet wakefulness as opposed to grooming, for the population.

Here, light stimulation consisted of 1-s epochs of 30-Hz square pulses with a 5-ms pulse width, followed by a 4-s inter-stimulation interval. An example recording (shown in Figure 4A) documents LFP spectral peaks at 30, 60, and 90 Hz, corresponding to the first 3 harmonics of the optical stimulation frequency. Across the population of rats analyzed (N = 4,; ChR2: recording sites 1–6, Chronos: recording sites 7–10), we found that spectral enhancements at 30 and 60 Hz tended to vary somewhat between animals, but each animal studied exhibited a significant peak at 1 of the 2 frequencies (see Figure 4B). In addition, an unpaired t test with Welch correction revealed no difference in the increase of either 30 or 60 Hz peaks between the Chronos and ChR2 stimulated animals (30 Hz: $t(3.203) = 2.28$, $p = 0.1013$; 60 Hz: $t(3.42) = 0.344$, $p = 0.7509$).

While the stimulation evoked narrow band peaks, we also observed a broadband BF LFP gamma peak in the object training session T4 during optical BF PV stimulation, as illustrated for an example session in Figure 4C. This gamma activity, which we have previously described in rat BF (Nair et al., 2018), is endogenous and unrelated to the PV stimulation. Consistent with previous reports, broadband gamma was suppressed during exploration compared to both quiet wakefulness and grooming

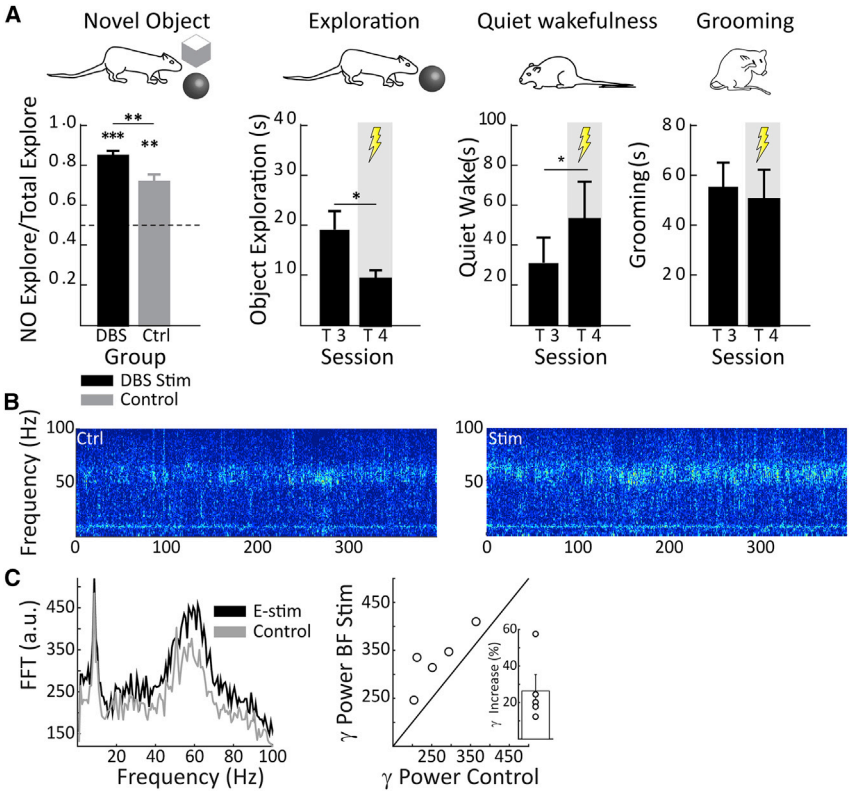

Figure 5. Effects of BF Electrical Stimulation on Performance and Behavior during a NOR Test

(A) The structure of the novel object task was identical as to that illustrated in Figure 4A; however, on T4, instead of BF PV optical stimulation, animals received BF electrical stimulation, as described in Method Details, and control animals received no stimulation. Both groups spent significantly more time with the novel object, as shown in the left-most panel, but the animals that received electrical BF stimulation on the prior day spent significantly more time with the NO than the control group. BF electrical stimulation also reduced exploratory behavior and concurrently increased periods of quiet wakefulness (center 2 panels), but had no effect on the time that the animals spent grooming (right panel).

(B) Single-session spectrogram of BF LFP activity in the NOR arena during stim off (left panel) and stim on epochs condition (right panel) for a representative animal, showing that during stimulation, broadband gamma activity increased; note that stimulation epochs have been removed for clarity.

(C) The left panel shows an example FFT during electrical stimulation (black lines) and control epochs (gray lines), revealing an increase in broadband gamma power during electrical stimulation. This was true for the population, as shown in the right panel, with the inset summarizing the magnitude of the increased power versus control epochs for all of the animals. Error bars reflect +/− SEM.

across recordings (quiet: $t(16) = 3.592$, $p = 0.0024$; grooming: $t(16) = 8.791$, $p < 0.0001$). As also reported previously, broadband gamma power (40–80 Hz) was greater during grooming than during quiet wakefulness ($t(16) = 7.888$, $p < 0.0001$; see Figure 4D). Our previous results document that elevated gamma power occurs not only in the BF but also in the ACC, an important cortical node of the DMN. Here, we replicate this finding and expand it to include multiple recording sites across the extent of the medial cortical mantle that constitute the rat DMN, including two sites located in the retrosplenial cortex (see Figure S1). We demonstrate that resting state-related gamma modulations occur across these recording sites, supporting the idea that BF coordinates not only ACC activity but also activity more generally across the DMN. In addition, we demonstrate here that the optogenetic activation of BF PV neurons enhances the interareal coupling of gamma fluctuations across DMN nodes (2-way ANOVA [$F(1,18) = 4.4$, $p < 0.05$], with no difference between nodes [$F(2,18) = 0.32$, $p > 0.5$]; see Figure S2). We noticed a novel aspect of gamma regulation related to behavioral state in these data, namely, that gamma peak frequency was lower for grooming than for quiet wakefulness (paired t test: $t(16) = 3.142$, $p = 0.0063$; see Figure 4E). These results indicate a shift in gamma power toward higher frequencies during quiet wakefulness as compared to grooming, suggesting that partially distinct but overlapping neural circuits may underlie the generation of these two behaviors.

The above results detail the effects of the specific upregulation of PV neurons in the BF. Given the fact that BF neurons of distinct cell types tend to be highly reciprocally connected and activated in a coordinated manner (Zaborszky and Duque, 2000), we tested what the effect might be of a more global, non-cell-type-specific activation of the BF on memory encoding and DMN-related behaviors. We used electrical deep brain stimulation (DBS) to activate BF neuronal circuits and investigated the behavior of rats in the same NOR paradigm described above, as illustrated in Figure 3A. We validated the NOR test by showing that both DBS-stimulated and non-stimulated control animals exhibited a significant novelty preference (DBS: $t(5) = 14.84$, $p < 0.0001$; control: $t(5) = 6.878$, $p = 0.0010$; see Figure 5A), indicating that both groups of animals were able to discriminate familiar objects from novel ones during the test session. Unlike the BF PV-stimulated rats, the BF DBS-stimulated animals showed an enhancement of memory encoding in the NOR test, with the novelty preference ratio for the DBS-stimulated animals being significantly higher than for controls ($t(5) = 3.324$, $p = 0.0209$). As we did for the PV-stimulated group, we assessed how BF DBS affected behavior during electrical stimulation by comparing the prevalence of behaviors of interest in object training sessions T3 and T4 for stimulated and control animals. Object exploration time was decreased during BF DBS ($t(5) = 3.685$, $p = 0.0142$), but unchanged in the control group ($t(5) = 1.335$, $p = 0.2393$; see Figure 5A). This effect is similar to what we observed in the PV-stimulated animals, suggesting that decreased exploratory behavior may in fact involve PV activation. Examining DMN-type behaviors, we found that grooming was unaffected by BF DBS stimulation (DBS group: $t(5) =$

0.6719, p = 0.5314; control group: t(5) = 0.3672, p = 0.7285), whereas the amount of time that the rats spent in a state of quiet wakefulness was significantly increased by BF DBS (DBS group: t(5) = 3.063, p = 0.0280; control group: t(5) = 2.218, p = 0.0773). Thus, while both BF DBS and BF PV stimulation enhanced DMN-type behaviors, the specific behaviors differed between the two stimulation methods, probably due to the recruitment of distinct but overlapping neural circuits. This idea is further supported by examining how the BF LFP is affected by DBS. Similar to BF PV stimulation, BF DBS enhanced gamma band LFPs in the BF, as illustrated in Figure 5B for a representative animal during stimulation and control conditions. However, while PV optical activation induced narrow band gamma power at stimulation frequency and harmonics during stimulation (see Figure 4A), DBS-induced broadband gamma power increases (see Figure 5C) and did so significantly across experiments ($p < 0.001$; Figure 5C).

The above findings, together with the previous literature, suggest that BF circuits are involved in memory consolidation and in the regulation of DMN-type behaviors, involving neurotransmitters systems, including GABA and acetylcholine (Ach). Neural communication, however, is not solely dependent on amino acid neurotransmitters and neuromodulators, but also involves neuropeptides, a broad class of bioactive molecules that are often co-released by neurons during activity and potentially contribute to brain-state regulation. We therefore used quantitative mass spectrometry to examine how BF DBS affected the local expression of neuropeptides. For these studies, animals received multiple BF DBS sessions, as illustrated in Figure 6A. Briefly, animals received 3 daily sessions of DBS consisting of three 1-h stimulation epochs separated by 1-h epochs where no stimulation was delivered. Stimulation epochs themselves consisted of 500-ms-long trains of 20 Hz followed by 10 s of no stimulation (see Method Details). Immediately following the final stimulation session, brain samples from the BF and two additional cortical brain areas, the ACC and the VC, were extracted and prepared for analytical liquid chromatography-mass spectrometry (see Method Details). We identified neuropeptides from BF, ACC, and VC samples. Focusing first on the BF, we found that DBS produced significant changes in 31 neuropeptides, mainly derived from 7 precursors (see Figure 6B; Table 1). We observed both up- and downregulation of individual neuropeptides, with members of a given peptide family tending to be modulated in the same direction. While BF DBS strongly affected the regulation of peptides locally in the BF, we also observed an impact of BF DBS on distant brain regions and, in particular, in the cortical areas ACC and VC that we targeted for analysis here (see Table 1). We found that in the VC, the regulation of 11 peptides were affected by BF DBS, a number of which were also modulated in BF. Of these, some were modulated in the same direction in both areas, such as members of the proenkephalin and secretogranin families, whereas other peptides, including members of the thymosin and VGF families were modulated in the opposite direction. While peptide levels in both BF and VC were thus affected by BF DBS, regulation in the two brain structures appeared to differ based on the analysis of the significantly modulated peptides. To examine this apparent dissociation in peptide regulation, we compared the BF DBS-induced change in neuropeptide levels in the VC, ACC, and BF for all of the peptides that were reliably detected in all three brain areas studied (see Figure 6C). We found that the neuropeptide modulation was uncorrelated between VC and BF ($r = -0.1751$, $p = 0.1228$), suggesting that while BF DBS does trigger gene expression and release of bioactive molecules in the VC, these modulations are distinct from those occurring within the BF. This is in stark contrast to the relation between BF and ACC peptide expression: peptide regulation was more specific within the ACC, with only two peptides significantly modulated, and both of these were modulated in the same direction as members of the same family within the BF. Furthermore, neuropeptide modulation between BF and ACC was positively correlated ($r = 0.3175$, $p = 0.0044$; Figure 6C), consistent with the idea that the BF and the ACC are part of a functionally coupled network (i.e., the DMN). It is important to remember that BF DBS likely activates projections both to DMN structures and to sensory cortical areas such as the VC. The peptide correlation analysis is consistent with this, as it reveals an impact of BF DBS on both of these cortical targets.

DISCUSSION

The DMN is a collection of cortical brain regions, including notably medial, frontal, and parietal structures (Lu et al., 2012; Raichle, 2015; Stafford et al., 2014), that are coherently active during internally focused cognitive states in which attention is withdrawn from the external environment. During natural behavior, periods of DMN activation alternate with periods of externally focused attention, when the dorsal attention network (DAN) is activated (Fox et al., 2005). Since DMN and DAN activation do not co-occur, the brain must switch from one state to the other. Our findings provide causal evidence for an important role of the BF PV neural population in triggering state switching by activating the DMN brain state and associated behaviors.

Using optogenetic activation of BF PV neurons, we present two items of behavioral evidence as well as electrophysiological evidence implicating the BF in DMN brain state transitions. During the NOR task, BF PV neuron activation enhances BF gamma oscillations at the stimulation frequency and reduces familiar object exploration time. Similarly, retrieval latency of a visible food item increases following BF PV activation, which is consistent with a reduced tendency for explorative behavior. These findings are consistent with the well-established suppression of gamma band activity during attentional, explorative processing that characterizes the DMN structures (Kojima et al., 2009; Nair et al., 2018; Ossandón et al., 2011) and provide further evidence for the idea that the BF is indeed an important node of the DMN. Several studies have provided correlative evidence for an involvement of the BF in DMN-related state transitions. For example, fMRI studies in humans have highlighted robust functional connectivity between BF and cortical areas of the DMN (Alves et al., 2018, 2019; Markello et al., 2018). These findings thus provide structural evidence that is highly consistent with the functional impact of the BF on DMN areas reported in the present study. Furthermore, the BF exhibits a particularly high centrality among DMN member structures (Alves et al., 2018, 2019), potentially consistent with a role of the BF in actively

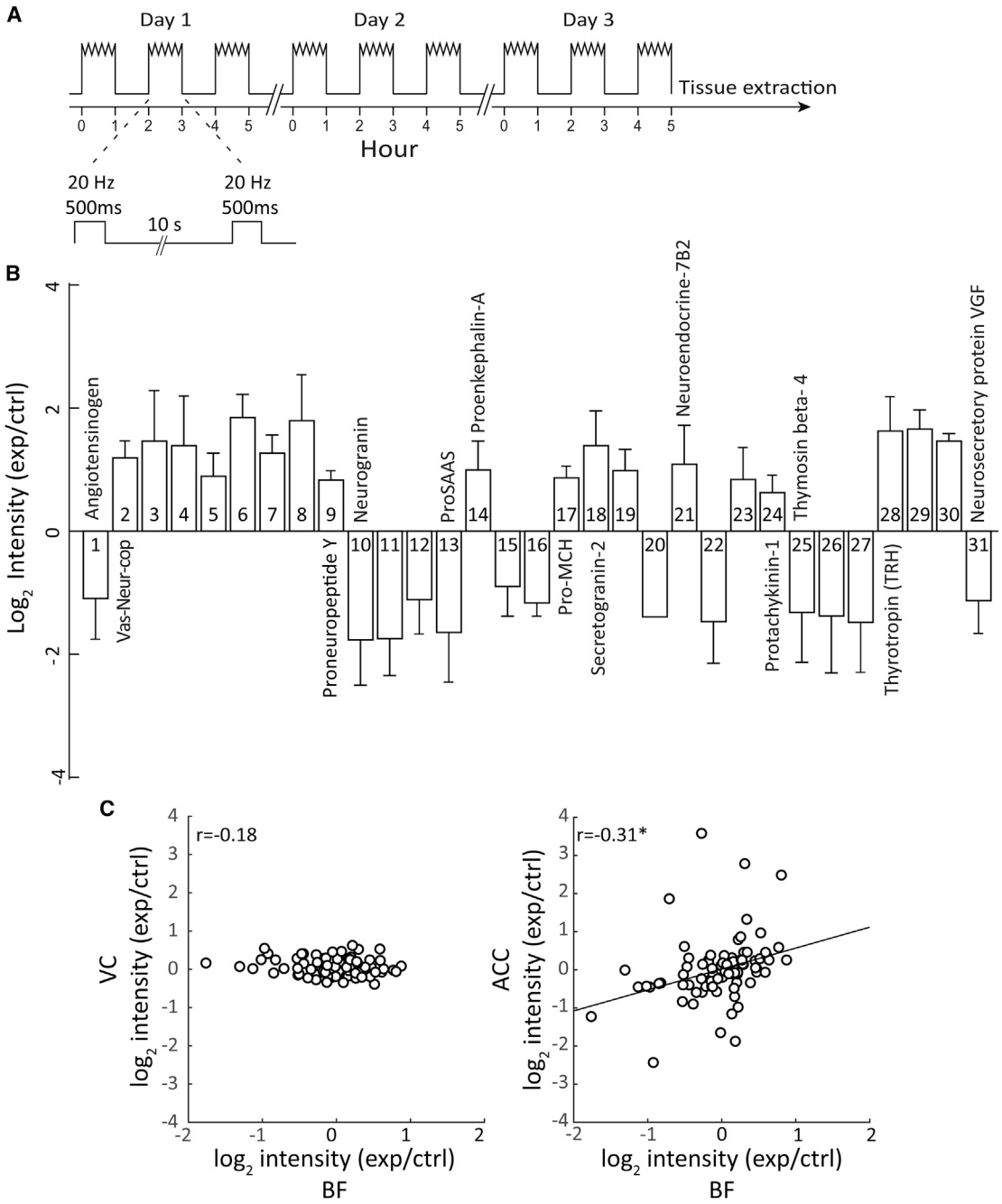

Figure 6. BF Electrical Stimulation Modulates Neuropeptide Levels within the BF and Specific Cortical Regions

(A) Schematic of the stimulation protocol.

(B) BF neuropeptides that showed significant modulation following BF electrical stimulation; increasers (upward bars), degreasers (downward bars). Neuropeptides are grouped by family (text above or below first family member in group). For example, all of the members of the Vasopressin Neurophysin2 copeptin1 (Vas-Neur-cop) family showed an increased intensity. The particular peptides are detailed in Table 1. Error bars reflect +/− SEM.

(C) We correlated the intensity of all of the BF neuropeptides detected, regardless of modulation, with the same peptides in VC (left panel), and the ACC (right panel). Neuropeptides were uncorrelated between BF and VC, but showed a significant correlation between BF and ACC.

triggering DMN state transitions. Simultaneous recordings from BF and the ACC, an important cortical DMN node, have not only described coherent oscillations among these two areas but also presented evidence for directional coupling from BF to cortex (Nair et al., 2016, 2018), also suggesting potential involvement of the BF in triggering state transitions. We show here that optical activation of BF PV neurons entrained the ACC LFP at the stimulation frequency, adding further evidence for BF-ACC

Table 1. Summary of Neuropeptide Changes in Three Brain Regions following DBS of the Basal Forebrain

Area	No. Increase (+) Decrease (−)	Precursor	Neuropeptide	Gene	ID	Sequence
BF	1−	angiotensinogen	–	Agt	P01015	GAEANLGKMG
	2+	vasopressin-neurophysin 2 copeptin	Arg-vasopressin	Avp	P01186	GTQESVDSAKPR
	3+	vasopressin-neurophysin 2 copeptin	Arg-vasopressin	Avp	P01186	LAGTQESVDSAKPR
	4+	vasopressin-neurophysin 2 copeptin	Arg-vasopressin	Avp	P01186	QLAGTQESVDSAKP
	5+	vasopressin-neurophysin 2 copeptin	Arg-vasopressin	Avp	P01186	QLAGTQESVDSAKPR
	6+	vasopressin-neurophysin 2 copeptin	Arg-vasopressin	Avp	P01186	QLAGTQESVDSAKPRVY
	7+	vasopressin-neurophysin 2 copeptin	Arg-vasopressin	Avp	P01186	VQLAGTQESVDSAKP
	8+	vasopressin-neurophysin 2 copeptin	Arg-vasopressin	Avp	P01186	VQLAGTQESVDSAKPR
	9+	pro-neuropeptide Y	neuropeptide Y	Npy	P07808	TENAPRTRLEDPSMW
	10−	neurogranin	–	Nrgn	Q04940	GPGPGGPGGAGGARGGAGGGP
	11−	neurogranin	–	Nrgn	Q04940	GPGPGGPGGAGGARGGAGGGPSGD
	12−	neurogranin	–	Nrgn	Q04940	GPGGPGGAGGARGGAGGGP
	13−	proSAAS	–	Pcsk1n	Q9QXU9	AVPRGEAAGAVQELARALAHLLE
	14+	proenkephalin-A	metenkephalin/ synenkephalin	Penk	P04094	SLPSDEEGESYSKEVPEME
	15−	proenkephalin-A	metenkephalin/ synenkephalin	Penk	P04094	VEPEEEANGGEILA
	16−	proenkephalin-A	metenkephalin/ synenkephalin	Penk	P04094	RPEWWMDYQ
	17+	pro-MCH	–	Pmch	P14200	NVEDDIVFNTFRMGKA
	18+	secretogranin-2	–	Scg2	P10362	IPKVAWIPDVE
	19+	secretogranin-2	–	Scg2	P10362	FQELGKLTGPSNQ
	20−	secretogranin-2	–	Scg2	P10362	ALPDGLSVEDILNVL
	21+	neuroendocrine protein 7B2	–	Scg5	P27682	VGPQSIEGGAHEGLQ
	22−	neuroendocrine protein 7B2	–	Scg5	P27682	SPRTPDRVSETDIQRLL
	23+	neuroendocrine protein 7B2	–	Scg5	P27682	GIARPRVEYPAHQAM
	24+	protachykinin-1	substance P/ neurokinin A/ neuropeptide K,γ	Tac1	P06767	MPEPFEHLL
	25−	thymosin β-4	–	Tmsb4x	P62329	NPLPSKETIE
	26−	thymosin β-4	–	Tmsb4x	P62329	NPLPSKETIEQEKQ
	27−	thymosin β-4	–	Tmsb4x	P62329	KNPLPSKETIEQEKQAGES
	28+	tyrotropin releasing Hormone	thyroliberin-releasing hormone	Trh	P01150	FPWMESDVT

(*Continued on next page*)

Table 1. *Continued*

Area	No. Increase (+) Decrease (–)	Precursor	Neuropeptide	Gene	ID	Sequence
	29+	tyrotropin releasing Hormone	thyroliberin-releasing hormone	Trh	P01150	LQRVRGDLGAALDSWIT
	30+	tyrotropin releasing Hormone	thyroliberin-releasing hormone	Trh	P01150	SWFSDVPQV
	31–	neurosecretory protein VGF	–	Vgf	P20156	APPEPVPPPRAA
VC	32–	chromogranin-A	–	Chga	P10354	QLAKELTAE
	33–	secretogranin-1	–	Chgb	O35314	HAAGESKDANVATANLGE
	34+	phosphatidyle thanolamine binding protein 1	–	Pebp1	P31044	HLGAPVAGTCF
	35+	phosphatidyle thanolamine binding protein 1	–	Pebp1	P31044	MNRPSSISWDGLDPGKLYTL
	36–	phosphatidyle thanolamine binding protein 1	–	Pebp1	P31044	GPLSLQEVDEPPQHALRV
	37–	proenkephalin-A	metenkephalin/ synenekephalin	Penk	P04094	LYPVEPEEEANGGEILA
	38+	proenkephalin-A	metenkephalin/ synenekephalin	Penk	P04094	VGRPEWWMDYQ
	39–	pro-MCH	–	Pmch	P14200	IGDEENSAKFPIG
	40+	neuroendocrine protein 7B2	–	Scg5	P27682	VGPQSIEGGAHEGLQH
	41+	thymosin beta-4	–	Tmsb4x	P62329	NPLPSKETIEQEKQAGES
	42+	thymosin beta-4	–	Tmsb4x	P62329	KNPLPSKETIEQEKQAGES
	43+	neurosecretory protein VGF	–	Vgf	P20156	APPGRSDVYPPP
ACC	44+	secretogranin-1	–	Chgb	O35314	GVAELDQLLHY
	45–	thymosin beta-10	–	Tmsb10	P63312	TLPTKETIEQEKRSEIS

coupling and directly implicating PV projection neurons in BF-ACC interactions. Further evidence along these lines comes from work in the macaque monkey, where transient BF local field potential activations in the BF in the gamma and other frequency ranges have been shown to precede fluctuations in cortical fMRI deflections (Liu et al., 2019).

In addition to reducing exploration behavior, we observed that animals spent increased amounts of time in a state of self-grooming during BF PV optogenetic stimulation. We consider that self-grooming, along with quiet wakefulness, are behaviors compatible with a DMN brain state, because they both occur during disengagement from external sensory processing and are both associated with elevated gamma oscillations in the BF (Nair et al., 2018). Furthermore, it has recently been shown that transient increases in activity in DMN structures may also be associated with large changes in cognitive context (Crittenden et al., 2015; Smith et al., 2019). This is particularly interesting when it comes to the issue of rodent grooming, which also tends to occur during state transitions—for example between protracted quiet and active states, such as sleep to wake or exploration to quiet (Bolles, 1960; Fentress, 1988). Thus, BF PV activation both reduces exploration and enhances one aspect of the DMN behavioral repertoire. This is consistent with evidence from recordings from identified single BF neurons, as BF GABAergic neurons encompass a population that is activated during self-grooming, although as a whole GABAergic neurons tend to exhibit mixed excitation and suppression during grooming and other behaviors (Harrison et al., 2016). However, exploration is well known to be associated with the consistently elevated activity of cholinergic BF neurons (Harrison et al., 2016; Hangya and Kepecs, 2015; Hassani et al., 2009). Interestingly, DBS BF stimulation also enhanced DMN-type behaviors—in this case, manifested by an increased amount of time spent in quiet wakefulness, as well as enhancing novelty preference on the day following the electrical activation, suggesting enhanced memory consolidation. DBS is not cell type specific, and we thus expect it to activate BF networks encompassing PV^+ and SST^+ GABAergic neurons, as well as glutamatergic and cholinergic populations (Záborszky et al., 2018). In line with previous studies linking cholinergic neuromodulation to improvements in learning and memory formation (see Hasselmo, 2006 for a review), we thus consider that the enhanced novelty preference triggered by BF DBS is likely due to cholinergic BF activation. However, we consider that the enhancement of quiet wakefulness

triggered by DBS may be due to the activation of GABAergic BF circuits. This is consistent with observations in the BF nucleus ventral pallidum, where optogenetic inhibition of SST GABAergic neurons triggers transitions from quiet wakefulness to exploratory behavior as well as enhances running speed (Espinosa et al., 2019a, 2019b). Available evidence thus points to an important role for BF GABAergic circuits in triggering DMN-type behaviors, with grooming and quiet wakefulness possibly involving preferential recruitment of PV and SST GABAergic populations.

We have demonstrated that BF optogenetic and electrical activation exerts a distinct causal influence promoting two types of DMN behavior, self-grooming and quiet wakefulness. The fact that gamma power in the BF is elevated in quiet states departs from observations in the hippocampus, where gamma power is positively correlated with running speed. In fact, in the BF, gamma activity seems to be unrelated to motor activity (Nair et al., 2018), suggesting different mechanisms underlying the entrainment of hippocampal and BF networks at gamma frequencies. While both of these behaviors are associated with robust BF gamma band activity, we have shown here that they possess distinct spectral signatures, perhaps indicating partially overlapping BF neural populations. We show here that while gamma oscillation peak frequency is lower for the grooming state than for the quiet state, gamma amplitude follows the opposite pattern, with higher values during grooming. At the same time, the overall upper envelope of endogenous gamma appears preserved across the two DMN-type behaviors. Our findings suggest that a population of GABAergic BF neurons are recruited during grooming, but not quiet wakefulness, generating larger overall amplitude at lower gamma frequencies. Alternatively the observed changes in gamma power and frequency may be related to intrinsic properties, such as GABAa (Buzsáki and Wang, 2012; Bartos et al., 2007) or GABAb (Kohl and Paulsen, 2010) receptor gating.

A notable aspect of our study is that we compare neural responses to optogenetic and electrical stimulation in the same brain area. PV-optogenetic activation at 30 Hz generated narrow-band distinct peaks in the LFP at stimulation frequency and harmonics, consistent with previous findings (Cardin et al., 2009; Kim et al., 2015). The narrow-band nature of the evoked activity is also limited temporally and does not extend much past the actual stimulation period. By contrast, electrical DBS activity is both broadband spectrally and has prolonged effects on network activity many seconds after stimulation offset. Thus, DBS appears to produce neural circuit activity much closer akin to endogenous oscillations than is the case for optogenetic activation. Note that while optogenetic stimulation with a randomized inter-stimulation interval does produce broader spectra, these remain punctate (Cardin et al., 2009; Kim et al., 2015) and remain distinct from endogenous gamma. Further studies examining the relation between DBS and optogenetics-related effects on neural circuit activity may be useful to disambiguate narrow- and broadband gamma modulations and their relation to behavior. We suggest that the BF regulation of DMN state orchestrates multiple aspects of task-off, internally focused behaviors and that this process involves multiple cell types and projection pathways, notably including but not limited to GABAergic projections. Our data are consistent with a role of the BF in switching from task-on to DMN brain states by activating neural projection systems dominated by cholinergic and GABAergic neurons, respectively. A co-activation of these two systems, which was likely triggered in our DBS experiments, may thus be uncharacteristic of the BF during natural behavior. A notable aspect of our study is that we assess how BF circuit activation affects neuropeptide expression within the BF as well as in cortical target structures of BF projections, including the ACC, an important DMN node, and as a control area, the VC, a sensory cortical structure considered to be part of the DAN. We discuss below a number of notable neuropeptides, whose expression is significantly modulated by BF DBS, first focusing on effects occurring locally within the BF. We found a significant decrease in angiotensinogen, a precursor of a number of neuropeptides, including angiotensin II, which has been implicated in several brain disorders including depression and neurodegeneration (Gard, 2004). The administration of angiotensin has been shown to produce deficits in memory acquisition and consolidation, and these deficits involve the depletion of ACh levels in the cortex or hippocampus (Tota et al., 2013), consistent with our findings of enhanced memory performance accompanied by decreased angiotensin precursor concentration. We identified seven peptides derived from arginine-vasopressin that were significantly upregulated by BF DBS. Available evidence indicates that arginine-vasopressin triggers episodes of self-grooming, followed by periods of immobility or quiet wakefulness (Meisenberg, 1988; Bielsky et al., 2004), which is consistent with our behavioral observations in the present study. Along similar lines, we found that the precursor of neuropeptide Y, another peptide previously linked to the initiation of self-grooming behavior in the BF (Tóth et al., 2007), was also upregulated following BF DBS. Finally, we also observed significant increases in protachykinin-1, the precursor of the neuropeptide substance P, for which a role in promoting memory formation has been documented with a site of action in the BF (Huston and Hasenöhrl, 1995). BF DBS upregulates multiple peptides associated with DMN-type behaviors (i.e., inducing quiet wakeful state or self-grooming), while at the same time, several peptides known to promote memory formation are also affected. These findings are highly consistent with the behavioral effects of BF DBS, which enhance both quiet wakefulness and memory consolidation. Monitoring neuropeptide changes following causal interventions shows that the triggering and maintenance of brain states, in addition to the circuit activity of classical neurotransmitters and neuromodulators, may critically depend on the synthesis and release of neuropeptides. The correlation in peptide regulation between BF and DMN node ACC provides further support for the idea that the BF is a key subcortical node of the DMN, which is consistent with electrophysiological and other functional evidence from our lab and others.

In summary, we provide multiple lines of evidence for a causal role of the BF in triggering transitions to the default brain state, implicating in particular the PV GABAergic neural population. We suggest that the BF coordinates activity in DMN cortical brain areas by regulating neural circuit activity through axonal corticopetal projections and modulating neuropeptide expression. Our findings suggest that the role of the BF is multifaceted, far beyond

the well-established role of the BF cholinergic system as promoting attention and arousal. Close proximity between attention-promoting cholinergic and DMN-promoting GABAergic circuits may be key to the initiation and maintenance of distinct and complementary cortical states.

STAR★METHODS

Detailed methods are provided in the online version of this paper and include the following:

- KEY RESOURCES TABLE
- RESOURCE AVAILABILITY
  - Lead Contact
  - Materials Availability
  - Data and Code Availability
- EXPERIMENTAL MODEL AND SUBJECT DETAILS
  - *Animals*
- METHOD DETAILS
  - Viral Injections
  - Implantation of optic fibers and electrodes
  - Whole Cell Patch Recordings
  - Electrophysiology
  - Optical Stimulation
  - Deep Brain Stimulation (DBS)
  - Surface food test
  - Novel object recognition (NOR) protocol
  - Histology and microscopy
  - Mass spectrometry analysis, sample preparation
  - LC-MS data acquisition
- QUANTIFICATION AND STATISTICAL ANALYSIS

SUPPLEMENTAL INFORMATION

Supplemental Information can be found online at https://doi.org/10.1016/j.celrep.2020.108359.

ACKNOWLEDGMENTS

This work was supported by Swiss National Science Foundation grant no. SNF 182504, to G.R.

AUTHOR CONTRIBUTIONS

L.L.-M., M.H., R.S., and G.R. designed the experiments. L.L.-M., M.D., R.M., W.L., M.K., M.H., and G.R. analyzed the data. L.L.-M., M.D., R.M., W.L., J.N., and M.K. conducted the experiments. L.L.-M., M.H., and G.R. wrote the paper.

DECLARATION OF INTERESTS

The authors declare no competing interests.

Received: November 27, 2019
Revised: May 25, 2020
Accepted: October 16, 2020
Published: November 10, 2020

REFERENCES

Alitto, H.J., and Usrey, W.M. (2003). Corticothalamic feedback and sensory processing. Curr. Opin. Neurobiol. *13*, 440–445.

Alves, P.N., Foulon, C., Cerliani, L., Karolis, S., and Thiebaut De Schotten, M. (2018). Subcortical anatomy of the default mode network: a functional and structural connectivity study. Eur. J. Neurol. *25*, 673.

Alves, P.N., Foulon, C., Karolis, V., Bzdok, D., Margulies, D.S., Volle, E., and Thiebaut de Schotten, M. (2019). An improved neuroanatomical model of the default-mode network reconciles previous neuroimaging and neuropathological findings. Commun. Biol. *2*, 370.

Antunes, M., and Biala, G. (2012). The novel object recognition memory: neurobiology, test procedure, and its modifications. Cogn. Process. *13*, 93–110.

Bartos, M., Vida, I., and Jonas, P. (2007). Synaptic mechanisms of synchronized gamma oscillations in inhibitory interneuron networks. Nat. Rev. Neurosci. *8*, 45–56.

Baxter, M.G., and Chiba, A.A. (1999). Cognitive functions of the basal forebrain. Curr. Opin. Neurobiol. *9*, 178–183.

Bhattacharyya, A., Bießmann, F., Veit, J., Kretz, R., and Rainer, G. (2012). Functional and laminar dissociations between muscarinic and nicotinic cholinergic neuromodulation in the tree shrew primary visual cortex. Eur. J. Neurosci. *35*, 1270–1280.

Bhattacharyya, A., Veit, J., Kretz, R., Bondar, I., and Rainer, G. (2013). Basal forebrain activation controls contrast sensitivity in primary visual cortex. BMC Neurosci. *14*, 55.

Bielsky, I.F., Hu, S.B., Szegda, K.L., Westphal, H., and Young, L.J. (2004). Profound impairment in social recognition and reduction in anxiety-like behavior in vasopressin V1a receptor knockout mice. Neuropsychopharmacology *29*, 483–493.

Boersema, P.J., Raijmakers, R., Lemeer, S., Mohammed, S., and Heck, A.J. (2009). Multiplex peptide stable isotope dimethyl labeling for quantitative proteomics. Nat. Protoc. *4*, 484–494.

Bolles, R.C. (1960). Grooming behavior in the rat. J. Comp. Physiol. Psychol. *53*, 306–310.

Buzsáki, G., and Wang, X.J. (2012). Mechanisms of gamma oscillations. Annu. Rev. Neurosci. *35*, 203–225.

Cardin, J.A., Carlén, M., Meletis, K., Knoblich, U., Zhang, F., Deisseroth, K., Tsai, L.H., and Moore, C.I. (2009). Driving fast-spiking cells induces gamma rhythm and controls sensory responses. Nature *459*, 663–667.

Chamoun, M., Groleau, M., Bhat, M., and Vaucher, E. (2016). Dose-dependent effect of donepezil administration on long-term enhancement of visually evoked potentials and cholinergic receptor overexpression in rat visual cortex. J. Physiol. Paris *110*, 65–74.

Crittenden, B.M., Mitchell, D.J., and Duncan, J. (2015). Recruitment of the default mode network during a demanding act of executive control. eLife *4*, e06481.

De Luna, P., Veit, J., and Rainer, G. (2017). Basal forebrain activation enhances between-trial reliability of low-frequency local field potentials (LFP) and spiking activity in tree shrew primary visual cortex (V1). Brain Struct. Funct. *222*, 4239–4252.

Do, J.P., Xu, M., Lee, S.H., Chang, W.C., Zhang, S., Chung, S., Yung, T.J., Fan, J.L., Miyamichi, K., Luo, L., and Dan, Y. (2016). Cell type-specific long-range connections of basal forebrain circuit. eLife *5*, e13214.

Dotigny, F., Ben Amor, A.Y., Burke, M., and Vaucher, E. (2008). Neuromodulatory role of acetylcholine in visually-induced cortical activation: behavioral and neuroanatomical correlates. Neuroscience *154*, 1607–1618.

Espinosa, N., Alonso, A., Lara-Vasquez, A., and Fuentealba, P. (2019a). Basal forebrain somatostatin cells differentially regulate local gamma oscillations and functionally segregate motor and cognitive circuits. Sci. Rep. *9*, 2570.

Espinosa, N., Alonso, A., Morales, C., Espinosa, P., Chávez, A.E., and Fuentealba, P. (2019b). Basal Forebrain Gating by Somatostatin Neurons Drives Prefrontal Cortical Activity. Cereb. Cortex *29*, 42–53.

Fentress, J.C. (1988). Expressive contexts, fine structure, and central mediation of rodent grooming. Ann. N Y Acad. Sci. *525*, 18–26.

Fox, M.D., Snyder, A.Z., Vincent, J.L., Corbetta, M., Van Essen, D.C., and Raichle, M.E. (2005). The human brain is intrinsically organized into dynamic, anticorrelated functional networks. Proc. Natl. Acad. Sci. USA *102*, 9673–9678.

Gard, P.R. (2004). Angiotensin as a target for the treatment of Alzheimer's disease, anxiety and depression. Expert Opin. Ther. Targets *8*, 7–14.

Gaskin, S., Tardif, M., Cole, E., Piterkin, P., Kayello, L., and Mumby, D.G. (2010). Object familiarization and novel-object preference in rats. Behav. Processes *83*, 61–71.

Goard, M., and Dan, Y. (2009). Basal forebrain activation enhances cortical coding of natural scenes. Nat. Neurosci. *12*, 1444–1449.

Greicius, M.D., Krasnow, B., Reiss, A.L., and Menon, V. (2003). Functional connectivity in the resting brain: a network analysis of the default mode hypothesis. Proc. Natl. Acad. Sci. USA *100*, 253–258.

Hangya, B., and Kepecs, A. (2015). Vision: how to train visual cortex to predict reward time. Curr. Biol. *25*, R490–R492.

Harris, K.D., and Thiele, A. (2011). Cortical state and attention. Nat. Rev. Neurosci. *12*, 509–523.

Harrison, T.C., Pinto, L., Brock, J.R., and Dan, Y. (2016). Calcium Imaging of Basal Forebrain Activity during Innate and Learned Behaviors. Front. Neural Circuits *10*, 36.

Hassani, O.K., Lee, M.G., Henny, P., and Jones, B.E. (2009). Discharge profiles of identified GABAergic in comparison to cholinergic and putative glutamatergic basal forebrain neurons across the sleep-wake cycle. J. Neurosci. *29*, 11828–11840.

Hasselmo, M.E. (2006). The role of acetylcholine in learning and memory. Curr. Opin. Neurobiol. *16*, 710–715.

Herrero, J.L., Roberts, M.J., Delicato, L.S., Gieselmann, M.A., Dayan, P., and Thiele, A. (2008). Acetylcholine contributes through muscarinic receptors to attentional modulation in V1. Nature *454*, 1110–1114.

Hsieh, C.Y., Cruikshank, S.J., and Metherate, R. (2000). Differential modulation of auditory thalamocortical and intracortical synaptic transmission by cholinergic agonist. Brain Res. *880*, 51–64.

Hsu, L.M., Liang, X., Gu, H., Brynildsen, J.K., Stark, J.A., Ash, J.A., Lin, C.P., Lu, H., Rapp, P.R., Stein, E.A., and Yang, Y. (2016). Constituents and functional implications of the rat default mode network. Proc. Natl. Acad. Sci. USA *113*, E4541–E4547.

Huston, J.P., and Hasenöhrl, R.U. (1995). The role of neuropeptides in learning: focus on the neurokinin substance P. Behav. Brain Res. *66*, 117–127.

Kalenscher, T., Lansink, C.S., Lankelma, J.V., and Pennartz, C.M. (2010). Reward-associated gamma oscillations in ventral striatum are regionally differentiated and modulate local firing activity. J. Neurophysiol. *103*, 1658–1672.

Kang, J.I., and Vaucher, E. (2009). Cholinergic pairing with visual activation results in long-term enhancement of visual evoked potentials. PLOS ONE *4*, e5995.

Kang, J.I., Groleau, M., Dotigny, F., Giguère, H., and Vaucher, E. (2014). Visual training paired with electrical stimulation of the basal forebrain improves orientation-selective visual acuity in the rat. Brain Struct. Funct. *219*, 1493–1507.

Kim, T., Thankachan, S., McKenna, J.T., McNally, J.M., Yang, C., Choi, J.H., Chen, L., Kocsis, B., Deisseroth, K., Strecker, R.E., et al. (2015). Cortically projecting basal forebrain parvalbumin neurons regulate cortical gamma band oscillations. Proc. Natl. Acad. Sci. USA *112*, 3535–3540.

Kimura, F., Fukuda, M., and Tsumoto, T. (1999). Acetylcholine suppresses the spread of excitation in the visual cortex revealed by optical recording: possible differential effect depending on the source of input. Eur. J. Neurosci. *11*, 3597–3609.

Kirschfeld, K. (1992). Oscillations in the insect brain: do they correspond to the cortical gamma-waves of vertebrates? Proc. Natl. Acad. Sci. USA *89*, 4764–4768.

Kohl, M.M., and Paulsen, O. (2010). The roles of GABAB receptors in cortical network activity. Adv. Pharmacol. *58*, 205–229.

Kojima, T., Onoe, H., Hikosaka, K., Tsutsui, K., Tsukada, H., and Watanabe, M. (2009). Default mode of brain activity demonstrated by positron emission tomography imaging in awake monkeys: higher rest-related than working memory-related activity in medial cortical areas. J. Neurosci. *29*, 14463–14471.

Lachaux, J.P., George, N., Tallon-Baudry, C., Martinerie, J., Hugueville, L., Minotti, L., Kahane, P., and Renault, B. (2005). The many faces of the gamma band response to complex visual stimuli. Neuroimage *25*, 491–501.

Laplante, F., Morin, Y., Quirion, R., and Vaucher, E. (2005). Acetylcholine release is elicited in the visual cortex, but not in the prefrontal cortex, by patterned visual stimulation: a dual in vivo microdialysis study with functional correlates in the rat brain. Neuroscience *132*, 501–510.

Liu, C., Yen, C.C., Szczupak, D., Ye, F.Q., Leopold, D.A., and Silva, A.C. (2019). Anatomical and functional investigation of the marmoset default mode network. Nat. Commun. *10*, 1975.

Lu, H., Zou, Q., Gu, H., Raichle, M.E., Stein, E.A., and Yang, Y. (2012). Rat brains also have a default mode network. Proc. Natl. Acad. Sci. USA *109*, 3979–3984.

Markello, R.D., Spreng, R.N., Luh, W.M., Anderson, A.K., and De Rosa, E. (2018). Segregation of the human basal forebrain using resting state functional MRI. Neuroimage *173*, 287–297.

Mathiasen, J.R., and Dicamillo, A. (2010). Novel object recognition in the rat: a facile assay for cognitive function. Curr. Protoc. Pharmacol., Chapter 5:Unit 5.59.

McKenna, J.T., Yang, C., Franciosi, S., Winston, S., Abarr, K.K., Rigby, M.S., Yanagawa, Y., McCarley, R.W., and Brown, R.E. (2013). Distribution and intrinsic membrane properties of basal forebrain GABAergic and parvalbumin neurons in the mouse. Journal of Comparative Neurology *521*, 1225–1250.

Meisenberg, G. (1988). Vasopressin-induced grooming and scratching behavior in mice. Ann. N Y Acad. Sci. *525*, 257–269.

Mesulam, M.M., Mufson, E.J., Wainer, B.H., and Levey, A.I. (1983). Central cholinergic pathways in the rat: an overview based on an alternative nomenclature (Ch1-Ch6). Neuroscience *10*, 1185–1201.

Munoz, J., Low, T.Y., Kok, Y.J., Chin, A., Frese, C.K., Ding, V., Choo, A., and Heck, A.J. (2011). The quantitative proteomes of human-induced pluripotent stem cells and embryonic stem cells. Mol. Syst. Biol. *7*, 550.

Nair, J., Klaassen, A.L., Poirot, J., Vyssotski, A., Rasch, B., and Rainer, G. (2016). Gamma band directional interactions between basal forebrain and visual cortex during wake and sleep states. J. Physiol. Paris *110*, 19–28.

Nair, J., Klaassen, A.-L., Arato, J., Vyssotski, A.L., Harvey, M., and Rainer, G. (2018). Basal forebrain contributes to default mode network regulation. Proc. Natl. Acad. Sci. USA *115*, 1352–1357.

O'Shea, J.P., Chou, M.F., Quader, S.A., Ryan, J.K., Church, G.M., and Schwartz, D. (2013). pLogo: a probabilistic approach to visualizing sequence motifs. Nat. Methods *10*, 1211–1212.

Oh, Y.-M., Karube, F., Takahashi, S., Kobayashi, K., Takada, M., Uchigashima, M., Watanabe, M., Nishizawa, K., Kobayashi, K., and Fujiyama, F. (2017). Using a novel PV-Cre rat model to characterize pallidonigral cells and their terminations. Brain Struct. Funct. *222*, 2359–2378.

Ossandón, T., Jerbi, K., Vidal, J.R., Bayle, D.J., Henaff, M.A., Jung, J., Minotti, L., Bertrand, O., Kahane, P., and Lachaux, J.P. (2011). Transient suppression of broadband gamma power in the default-mode network is correlated with task complexity and subject performance. J. Neurosci. *31*, 14521–14530.

Petruzziello, F., Falasca, S., Andren, P.E., Rainer, G., and Zhang, X. (2013). Chronic nicotine treatment impacts the regulation of opioid and non-opioid peptides in the rat dorsal striatum. Mol. Cell. Proteomics *12*, 1553–1562.

Pinto, L., Goard, M.J., Estandian, D., Xu, M., Kwan, A.C., Lee, S.H., Harrison, T.C., Feng, G., and Dan, Y. (2013). Fast modulation of visual perception by basal forebrain cholinergic neurons. Nat. Neurosci. *16*, 1857–1863.

Quinn, L.K., Nitz, D.A., and Chiba, A.A. (2010). Learning-dependent dynamics of beta-frequency oscillations in the basal forebrain of rats. Eur. J. Neurosci. *32*, 1507–1515.

Raichle, M.E. (2015). The brain's default mode network. Annu. Rev. Neurosci. *38*, 433–447.

Raichle, M.E., MacLeod, A.M., Snyder, A.Z., Powers, W.J., Gusnard, D.A., and Shulman, G.L. (2001). A default mode of brain function. Proc. Natl. Acad. Sci. USA *98*, 676–682.

Rappsilber, J., Mann, M., and Ishihama, Y. (2007). Protocol for micro-purification, enrichment, pre-fractionation and storage of peptides for proteomics using StageTips. Nat. Protoc. *2*, 1896–1906.

Ray, S., and Maunsell, J.H. (2015). Do gamma oscillations play a role in cerebral cortex? Trends Cogn. Sci. *19*, 78–85.

Sato, H., Hata, Y., Hagihara, K., and Tsumoto, T. (1987). Effects of cholinergic depletion on neuron activities in the cat visual cortex. J. Neurophysiol. *58*, 781–794.

Schwarz, A.J., Gass, N., Sartorius, A., Risterucci, C., Spedding, M., Schenker, E., Meyer-Lindenberg, A., and Weber-Fahr, W. (2013). Anti-correlated cortical networks of intrinsic connectivity in the rat brain. Brain Connect. *3*, 503–511.

Secher, A., Kelstrup, C.D., Conde-Frieboes, K.W., Pyke, C., Raun, K., Wulff, B.S., and Olsen, J.V. (2016). Analytic framework for peptidomics applied to large-scale neuropeptide identification. Nat. Commun. *7*, 11436.

Smith, V., Mitchell, D.J., and Duncan, J. (2019). The effect of rule retrieval on activity in the default mode network. Neuroimage *202*, 116088.

Soma, S., Shimegi, S., Osaki, H., and Sato, H. (2011). Cholinergic modulation of response gain in the primary visual cortex of the macaque. J. Neurophysiol. *107*, 283–291.

Stafford, J.M., Jarrett, B.R., Miranda-Dominguez, O., Mills, B.D., Cain, N., Mihalas, S., Lahvis, G.P., Lattal, K.M., Mitchell, S.H., David, S.V., et al. (2014). Large-scale topology and the default mode network in the mouse connectome. Proc. Natl. Acad. Sci. USA *111*, 18745–18750.

Svensson, M., Sköld, K., Nilsson, A., Fälth, M., Nydahl, K., Svenningsson, P., and Andrén, P.E. (2007). Neuropeptidomics: MS applied to the discovery of novel peptides from the brain. Anal. Chem. *79*, 15–16, 18–21.

Ting, J.T., Daigle, T.L., Chen, Q., and Feng, G. (2014). Acute brain slice methods for adult and aging animals: application of targeted patch clamp analysis and optogenetics. Methods Mol. Biol. *1183*, 221–242.

Tota, S., Goel, R., Pachauri, S.D., Rajasekar, N., Najmi, A.K., Hanif, K., and Nath, C. (2013). Effect of angiotensin II on spatial memory, cerebral blood flow, cholinergic neurotransmission, and brain derived neurotrophic factor in rats. Psychopharmacology (Berl.) *226*, 357–369.

Tóth, A., Hajnik, T., Záborszky, L., and Détári, L. (2007). Effect of basal forebrain neuropeptide Y administration on sleep and spontaneous behavior in freely moving rats. Brain Res. Bull. *72*, 293–301.

Turchi, J., and Sarter, M. (1997). Cortical acetylcholine and processing capacity: effects of cortical cholinergic deafferentation on crossmodal divided attention in rats. Brain Res. Cogn. Brain Res. *6*, 147–158.

Tyanova, S., Temu, T., and Cox, J. (2016a). The MaxQuant computational platform for mass spectrometry-based shotgun proteomics. Nat. Protoc. *11*, 2301–2319.

Tyanova, S., Temu, T., Sinitcyn, P., Carlson, A., Hein, M.Y., Geiger, T., Mann, M., and Cox, J. (2016b). The Perseus computational platform for comprehensive analysis of (prote)omics data. Nat. Methods *13*, 731–740.

Upadhyay, J., Baker, S.J., Chandran, P., Miller, L., Lee, Y., Marek, G.J., Sakoglu, U., Chin, C.L., Luo, F., Fox, G.B., and Day, M. (2011). Default-mode-like network activation in awake rodents. PLOS ONE *6*, e27839.

Vaz, R.P., Cardoso, A., Sá, S.I., Pereira, P.A., and Madeira, M.D. (2017). The integrity of the nucleus of the lateral olfactory tract is essential for the normal functioning of the olfactory system. Brain Struct. Funct. *222*, 3615–3637.

Witten, I.B., Steinberg, E.E., Lee, S.Y., Davidson, T.J., Zalocusky, K.A., Brodsky, M., Yizhar, O., Cho, S.L., Gong, S., Ramakrishnan, C., et al. (2011). Recombinase-driver rat lines: tools, techniques, and optogenetic application to dopamine-mediated reinforcement. Neuron *72*, 721–733.

Wonnacott, S. (1990). The paradox of nicotinic acetylcholine receptor upregulation by nicotine. Trends Pharmacol. Sci. *11*, 216–219.

Xu, M., Chung, S., Zhang, S., Zhong, P., Ma, C., Chang, W.-C., Weissbourd, B., Sakai, N., Luo, L., Nishino, S., and Dan, Y. (2015). Basal forebrain circuit for sleep-wake control. Nat. Neurosci. *18*, 1641–1647.

Zaborszky, L., and Duque, A. (2000). Local synaptic connections of basal forebrain neurons. Behav. Brain Res. *115*, 143–158.

Zaborszky, L., and Duque, A. (2003). Sleep-wake mechanisms and basal forebrain circuitry. Front. Biosci. *8*, d1146–d1169.

Zaborszky, L., Pang, K., Somogyi, J., Nadasdy, Z., and Kallo, I. (1999). The basal forebrain corticopetal system revisited. Ann. N Y Acad. Sci. *877*, 339–367.

Záborszky, L., Gombkoto, P., Varsanyi, P., Gielow, M.R., Poe, G., Role, L.W., Ananth, M., Rajebhosale, P., Talmage, D.A., Hasselmo, M.E., et al. (2018). Specific Basal Forebrain-Cortical Cholinergic Circuits Coordinate Cognitive Operations. J. Neurosci. *38*, 9446–9458.

Zhu, C., Yao, Y., Xiong, Y., Cheng, M., Chen, J., Zhao, R., Liao, F., Shi, R., and Song, S. (2017). Somatostatin neurons in the basal forebrain promote high-calorie food intake. Cell Rep. *20*, 112–123.

Zinke, W., Roberts, M.J., Guo, K., McDonald, J.S., Robertson, R., and Thiele, A. (2006). Cholinergic modulation of response properties and orientation tuning of neurons in primary visual cortex of anaesthetized Marmoset monkeys. Eur. J. Neurosci. *24*, 314–328.

STAR★METHODS

KEY RESOURCES TABLE

REAGENT or RESOURCE	SOURCE	IDENTIFIER
Antibodies		
Guniea pig anti PV antibody	Swant	RRID: AB_2665495
Donkey antiguinea pig Alexa 488	Jackson ImmunoResearch	Cat# 706-545-148
		Lo# 140967
		RRID: AB_2340472
Bacterial and Virus Strains		
AAV5-EF1aDIO-hChR2(H134R)mCherry-WPRE-Pa	University of North Carolina Vector Core	N/A
AAV5-EF1aDIO-mCherry (Control)	University of North Carolina Vector Core	N/A
AAV8-hSyn-FLEX-Chronos-GFP	University of North Carolina Vector Core	N/A
AAV5-EF1aDIO-EYFP-WPRE-Pa (Control)	University of North Carolina Vector Core	N/A
Deposited Data		
Raw and analyzed data	This paper	https://gin.g-node.org/RainerLab/PVDMN.git
Experimental Models: Organisms/Strains		
PV:Cre rats	Rat Resource and Research Center, University of Missouri, Columbia	LE-Tg (Pvalb-iCre)2Ottc
Software and Algorithms		
MATLAB	Mathworks, Natick, MA	N/A

RESOURCE AVAILABILITY

Lead Contact

Further information and requests for resources and reagents should be directed to and will be fulfilled by the Lead Contact, Gregor Rainer (gregor.rainer@unifr.ch).

Materials Availability

This study did not generate new unique reagents.

Data and Code Availability

The data reported in this paper are publicly available through the German neuroinformatics node, https://gin.g-node.org/RainerLab/PVDMN.git

EXPERIMENTAL MODEL AND SUBJECT DETAILS

Animals

The local ethical committee on animal experimentation (canton of Fribourg), approved all experimental procedures. A total of 29 male Long-Evans Rats, age 4-9 months, were used in this study. Of these there were 23 BAC transgenic rats expressing Cre recombinase under the rat parvalbumin (PV) promoter (LE-Tg (Pvalb-iCre)2Ottc, Rat Resource and Research Center, University of Missouri, Columbia) and 6 WT littermates. Animals were single housed on a 12 /12h light/dark cycle and had access to food and water *ad libitum.*

METHOD DETAILS

Viral Injections

Anesthesia was induced using 4% isoflurane and was maintained with 1%–2% isoflurane in pure O2 inhalation. Depth of anesthesia was frequently checked and adjusted such that the pedal withdrawal reflex was absent. Animals were placed in a stereotaxic device,

a midline incision was made on the scalp, and the periosteum was reflected. Two small burr holes were made over the left and right basal forebrain targets AP −0.6; ML ± 2.8, and a custom-made 26 gauge infuser was lowered to the target site (DV −8.6mm). One of 4 viral constructs (University of North Carolina Vector Core) were injected bilaterally: 1. 1 μL AAV5-EF1aDIO-hChR2(H134R)mCherry-WPRE-Pa, 5.2x10^{12} particles/ml; 2. 1 μL AAV5-EF1aDIO-mCherry (Control) 3.3 × 10^{12} particles/ml; 3. 0.5 μL AAV8-hSyn-FLEX-Chronos-GFP 4.6 × 10^{12} particles/ml; 4. AAV5-EF1aDIO-EYFP-WPRE-Pa (Control) 6.5 × 10^{12} particles/ml. Injections were made using a Hamilton syringe driven by a dual syringe pump (Kd Scientific, Holliston, MA) at 1 μL/min. The viral infuser was left in place for 10 minutes following each injection before it was slowly removed.

Implantation of optic fibers and electrodes

Four weeks after viral infusion was performed, animals underwent a second surgery to insert the optic fibers and optrodes into the BF (AP −0.6; ML ± 2.8; DV −8.5). Tungsten microelectrodes were implanted with a 10° medio-lateral angle into one of the BF hemispheres (AP −0.6; ML +4.4; DV; −9.2) and in the ACC (AP 3.7; ML ± 0.8; DV −2.4). The implanted optic fibers (240 μm outer diameter; Doric lenses), customized optrodes (240 μm optic fibers glued with two tungsten electrodes 50 μm; Doric lenses) and Tungsten microelectrodes (FHC Inc. Bowdoin ME, ∼400 kΩ) were secured to the skull surface with five stainless steel screws and dental cement. Four of these screws also served to monitor the EEG, 2 anterior screws (AP +2.7, ML ± 2.2) and 2 posterior screws (AP −6.5, ML ± 4). An additional screw over the cerebellum served as a reference. Electrodes and EEG screws were wired to a 10 pin connector. Four additional male PV-CRE rats, Figures S1 and S2, received bilateral BF injections of AAV5-EF1aDIO-hChR2(H134R)mCherry-WPRE-Pa. After a 1 week recovery, optrodes were implanted in the left and right BF, (AP −0.6; ML ± 2.8; DV −8.5). Additionally 2 ACC electrodes were implanted in the left hemisphere, ACC1&2 (AP 2.5 & AP 0.8; ML +1; DV −2.4). An RSC electrode was implanted, also in the left hemisphere RS1 (AP −2.9; ML +1; DV −1.9) and an additional stainless steel screw was implanted over RSC, left hemisphere RS2 (AP −4.4, ML + 1). All behavioral tests were conducted > 5 weeks post- viral injection and at least one week following optic fiber/electrode implantation. For electrical stimulation, tungsten microelectrodes (FHC Inc. Bowdoin ME) with tip resistances of ∼50 KΩ were implanted bilaterally in BF (AP- 0.8, ML ± 2.8, DV - 8.2). Additionally, a reference screw was placed on the midline over the cerebellum. Electrodes were connected to a 7-pin connector and fixed to the animal's skull using dental cement. All behavioral tests took place at least one week after electrode implantation.

Whole Cell Patch Recordings

To verify the function of Chronos in PV (+) MCPO neurons, patch-clamp electrophysiology was performed in acute slices from adult rats (7 weeks; protocol based on Ting et al. (2014). To this end, rats were injected with the AAV8-Chronos-GFP virus. Four weeks later, rats were anesthetized with 3% isoflurane in an induction chamber with fan system (Rothacher) and decapitated after the onset of anesthesia. The brain was quickly removed from the skull and placed in ice-cold dissection buffer (in mM): 110 NMDG (N-methyl-D-glutamine), 110 HCl, 2.5 KCl, 1.2 NaH_2PO_4, 25 $NaHCO_3$, 20 HEPES, 25 Glucose, 5 Sodium ascorbate, 2 Thiourea, 3 Sodium pyruvate, 10 $MgCl_2$, 0.5 $CaCl_2$, saturated with carbogen gas (95% O_2 and 5% CO_2). Coronal slices (300 μm) were cut using a Microtome VT1200S (Leica Microsystems). After the slicing procedure, brain sections containing the MCPO were placed for 7 min in heated dissection buffer (34°C) and afterward stored in HEPES based storage solution (in mM): 92 NaCl, 2.5 KCl, 30 $NaHCO_3$, 1.2 NaH_2PO_4, 20 HEPES, 25 Glucose, 5 Sodium ascorbate, 2 Thiourea, 3 sodium pyruvate, 2 MgCl2 and 2 CaCl2, at 34°C, pH7.4, saturated with carbogen, and allowed to cool down to room temperature.

Whole-cell patch-clamp recording was performed at room temperature in extracellular recording solution (in mM): 125 NaCl, 25 $NaHCO_3$, 2.5 KCl, 1.25 NaH_2PO_4, 1 $MgCl_2$, 2 $CaCl_2$, 10 glucose, 5 Sodium ascorbate, 2 Thiourea, 3 sodium pyruvate; using a EPC-10 patch-clamp amplifier (HEKA Elektronik) under the control of PatchMaster software (HEKA Elektronik). The patch pipette solution contained (in mM): 145 K-gluconate, 8 KCl, 10 HEPES, 5 EGTA, 3 Na_2Phosphocreatine, 4 MgATP, 0.3 Na_2GTP, at a pH of 7.2 (adjusted with KOH),∼300 mOsm. To test for light-evoked currents in GFP(-) and GFP(+) neurons, blue light pulses (1 ms) were applied from a high-power LED (CREE XP-E2, emission spectrum centered around λ = 480 nm; Cree Inc, USA) driven by a LED controller (Mightex BLS-1000-2). The LED light source was coupled into the epifluorescence port (TILLphotonics, Germany) of a BX51WI microscope (Olympus, Japan) equipped with the 60X / 0.9 NA objective. Current-clamp traces were analyzed using IgorPro using NeuroMatic plug-in.

Electrophysiology

Connectors on the head of PV:Cre rats were attached to a miniature wireless head stage (Multichannel Systems, Reutlingen Germany). Signals were acquired at 25 kHz, and data were stored on a PC for offline analysis. Connectors from DBS animals were attached to a miniature data logger (Neurologger 2A, Zurich Switzerland) equipped with an onboard accelerometer for monitoring movement, see Nair et al., 2016.

Optical Stimulation

A 200-μm patch cord was connected to the external portion of the chronically implantable optical fiber (Doric Lenses). Patch cords were attached to a 473-nm blue laser (Changchun New Industries Optoelectronics, China), and light pulses were controlled using a pulse generator, (Rigol, Beaverton OR). At the beginning of each experimental session laser intensity was adjusted to be within 6 to 9 mW using an optical power meter (PM 100D, Thorlabs Newton NJ). In all behavioral paradigms stimulation was delivered using 30 Hz

square pulses, 5 ms pulse width, for one second followed by a 4 s inter-stimulus interval. In an additional experiment estimating responses to different frequencies of stimulation a different stimulation protocol was used. In this case, animals received stimulation at 5 frequencies, (20, 30, 40, 50 and 60 Hz) with square pulses of a constant width of 10 ms. Stimuli were delivered for 5 s with a 10 s inter-stimulus interval.

Deep Brain Stimulation (DBS)

DBS was delivered using a custom made pulse generator. Pulse trains consisted of 8 Volt, 50 μs biphasic pulses at 20 Hz for 500 ms with an inter-train interval of 10 s, for behavioral experiments. For peptide studies pulse trains and inter-train intervals were identical as above, except trains were delivered continuously for three one hour bouts with an inter-bout interval of 1 hour, see Figure 6A.

Surface food test

In order to assess exploratory behavior a visible food test (Vaz et al., 2017) was performed on 3 Chronos injected animals and compared to 4 control animals injected with AAV8 empty virus and receiving identical optical stimulation. For reward familiarization, a highly palatable chocolate cereal was placed in the test chamber during two consecutive days before the test, and it was confirmed that that it was consumed by the rat. The chamber consisted of a clean standard plastic cage (36x 20x 29 cm) with new bedding material. After 20 h of food deprivation, the rat was placed in the chamber for 10 min to acclimate and BF PV stimulation at 30 Hz began. Then, without stopping the stimulation, the rat was removed from the cage and the palatable reward was placed on the surface of the bedding. The rat was re-introduced into the cage, while BF optical stimulation continued. The time spent to locate the palatable was measured as the latency between entrance to the chamber and the time the animal took the first bite of the food. The maximum test time allowed was 900 s. The animals behavior was recorded with a video camera (Logitech HD Webcam C270) and the video recordings were manually scored by an experimenter, naive to the rats treatment, using ELAN annotation software (ELAN 5.7). Latency to first bite of the palatable reward and time eating the palatable reward were scored.

Novel object recognition (NOR) protocol

A NOR task was performed to evaluates the rats' exploratory behaviors, recognition memory and 2 default mode like behaviors, grooming and quiet wakefulness. Two groups of animals were used, those that received ChR2-AAV5(N = 3) or Chronos-AAV8(N = 5) viral injections and a control group that received empty viral injections and received identical optical stimulation, (AAV5, N = 3; AAV8 N = 4).The paradigm consisted of three phases: arena habituation, object familiarization/training and memory recognition test, as previously described (Antunes and Biala, 2012). All behavioral sessions were carried out in the same open-field arena (60 × 60 × 40 cm3) made of black plastic walls and a metal grid floor. Rats were released from the side of the arena opposite to the objects, and the floor and walls were cleaned in between each session with diluted ethanol to avoid odor cues. The light intensity in the arena was ≈17 Lux, and white noise at 60dB was used in order to cover any background sounds. Videos were captured with a Genius WideCam F100 camera, and recordings were manually scored by an experimenter, naive to the rats treatment, using ELAN annotation software (ELAN 5.7). Durations of a set of behaviors were scored: Object exploration, arena exploration, grooming, and quiet wakefulness. In the habituation phase, each rat was allowed to freely explore the empty open-field arena. The schedule was the following: twice a day the animals were moved to the arena for a 10 minute session. This phase lasted for 4 days for a total of 8 sessions (H1 to H8), see Figure 3A. In between the two daily sessions, the animals were moved back to their home cage for 4-5 hours. Following habituation animals received 2 days of object training. Prior to the first training session two similar objects (by size, texture, and color) were placed in the arena. The animals were allowed to interact with these objects over two days twice a day for 10 minutes, with 4-5 hours in their home cages between sessions. (T1 to T4, Figure 3A). On the last training session, T4, animals received either BF PV optical stimulation or BF DBS. On the morning of day 7 a final 10 minute session was recorded with a novel object replacing one of the now familiar training objects (different shape, texture, size, and color). For optogenetic studies animals injected with empty viruses were used as controls, and opsin injected animals as the experimental group. For the DBS experiments rats were counterbalanced. After a 2week break, the whole paradigm was repeated with the prior experimental group now serving as controls and vice versa. A new set of novel and familiar objects were used for the second NOR test.

Histology and microscopy

Specificity of opsin (ChR2 and Chronos) coexpression in PV neurons, as well as viral injections and optic fiber placements were verified. Animals were transcardially perfused with 4% Paraformaldehyde (PFA) and decapitated, brains were rapidly isolated and transferred to a 4% PFA solution at 4°C for 24 h. Subsequently, the brains were transferred to a 30% sucrose solution at 4°C for 48 h. Then brains were frozen and stored at −20°C.

Detection of fluorophores (mCherry and GFP) and parvalbumin immunohistochemistry were performed in order to evaluate coexpression. Free-floating coronal sections of 40 μm were washed with TBS 0.1 M. Subsequently, brain sections were incubated in TBS 0.1M, 20% donkey serum, Guinea pig anti PV antibody (1:5,000 dilution, GP72, from Swant) over 72 hours at 4°C. Sections were then washed with TBS 0.1 M (2 times) and Tris (1 time); sections were then incubated with (1:200 Alexa 488 or Alexa 594 donkey antiguinea pig) for 3 h. Finally, sections were washed with Tris (2 times) and TBS 0.1M (1 time) and mounted onto microscope slides and coverslipped with Vectashield mounting medium that contained a DAPI nuclear counterstain (Reactolab SA). Viral expression

and fiber optic placement into the BF were checked in most of the rats used for behavioral experiments with the sliding microscope (Hamamatsu NanoZoomer). Only animals with sufficient viral expression and correct optic fiber placement within the BF were included in our study.

Co-localization study of viral injected cells and parvalbumin-positive (PV^+) in the BF was performed by using the Stereo Investigator system (Version 11, MicroBrightField, Williston, VT, USA). The system was connected to a Zeiss Axioplan microscope coupled with a Hamamatsu Orca Camera and with a motorized x-y stage (Ludl Electronic Products, LTD, NY, USA). Counting was done on images obtained with oil immersion objective lenses (x63 NA = 1.30). Six PV:Cre animals derived from heterozygous breedings were analyzed (3 animals receiving AAV5 injections and 3 animals with AAV8 injections). At each sampling location, the microscope was focused down through the dissector sample to count any cell within that particular counting frame according to dissector counting rules.

Mass spectrometry analysis, sample preparation

The neuropeptides extraction method was modified based on Petruzziello et al. (2013). The dimethyl label procedure was modified according to the previous protocol (Boersema et al., 2009; Munoz et al., 2011). To reduce interference peptides forming the fragmentations of proteins, restricted temperature controls were performed in the all extraction procedures after adding protease inhibitor Cocktail (Svensson et al., 2007). The BF, ACC and VC tissues are homogenized with 50 μL 8 M urea (pH 7.4) on Precellys 24 homogenizer (Bertin Technologies, Montigny-le-Bretonneux, France) twice within 1min, and then kept in ice bath for incubation 30 min. Another 250 μL of pure water was added into each sample and vortexed. The sample was centrifuged at 20,000 g for 1 h at 4°C and then the supernatant was collected. After extraction, the supernatant was filtered on a 10 kDa cutoff filter (Vivacon 500, Sartorious AG, Goettingen, Germany) by centrifuging for approximately 2 h at 14000 g at 4°C. The filtration was used for the dimethyl labeling procedure after adding 20 μL 1 M TEAB directly and gently vortexing for 10 s. Subsequently, we added 5 μL of 4% (v/v) CH_2O and $^{13}CD_2O$, 5 μL of 0.6 M $NaBH_3CN$ and $NaBD_3CN$ to the sample for ''light'' and ''heavy'' dimethyl labeling, respectively. The samples were incubated in a working fume hood for 45 min mixing slightly. Brief mixing occurred after every reagent addition at room temperature. Quenching of the labeling reaction was performed by adding 10 μL of 1% (v/v) ammonia solution and then acidifying the sample with 20 μL 0.2% formic acid. The differential labeled samples were mixed first and desalted with a C18 StageTip see Rappsilber et al. (2007), pre-washed with 200 μL 0.2% acetonitrile and 200 μL 0.2% formic acid in water twice, respectively. Finally, 200 μL of 80% acetonitrile containing 0.2% formic acid was used for eluting neuropeptide and then directly analysis by nanoLC-MS was performed with three replicates.

LC-MS data acquisition

The extracts were analyzed on Q Exactive coupled to EASY-nLC™ 1200 nanoflow-HPLC system (Thermo Fisher Scientific). Analytical column tips with 75 μm inner diameter (New Objective) were self-packed with 1.9 μm Reprosil-Pur C18 AQ (100Å, Dr. Maisch GmbH) to a length of 20 cm. No pre-column was used and samples were injected directly into the column. A gradient of A (0.5% formic acid (Fisher Scientific) in water) and B (0.1% formic acid in 80% ACN (Fisher Scientific) in water) with increasing organic proportion was used for peptide separation (loading sample with 2% B, separation ramp: from 10%–30% B within 80 min). The separation flow rate was 250 nL/min and for sample loading 800 nL/min. The mass spectrometry was operated in the data-dependent mode and switched automatically between MS (resolution 70,000, AGC $1e^6$) and MS/MS (resolution 17,500, AGC $1e^5$). Each MS scan was followed by a maximum of ten MS/MS scans with normalized collision energy 25%. Parent ions with a charge state of z = 1 and unassigned charge state were excluded for fragmentation. The mass range of MS was from 370 to 1750 m/z. The other mass spectrometry parameters were as follows: spay voltage 2.5 kV; no sheath and auxiliary gas flow; and ion-transfer tube temperature 200°C. Partially technical replicates were measured on Orbitrap Discovery (Thermo Fisher Scientific) coupled with UltiMate™ 3000 RSLCnano System (Thermo Fisher Scientific). The precolumn (μ-precolumn, C18 Pepmap, 300 μm ID, Thermo Scientific) was used for sample loading with 3 μL/min 100% A in a loading pump and then switched to the analytical column after 5 min. The 190 min gradient ramp from 2% to 30% B with flow rate 300 nL/min. The resolution was 30,000 for both MS (AGC $1e^6$) and MS/MS (AGC $2e^5$) with maximum top five. The fragmentation was performed in CID mode with a normalized collision energy of 35%. Only unassigned charge states of parent ions were excluded from fragmentation. The mass range of MS was from 400 to 1800 m/z. The other mass spectrometry and HPLC parameters used similar settings to the Q Exactive system.

QUANTIFICATION AND STATISTICAL ANALYSIS

LFPs were down-sampled to 1 kHz and were partitioned into 1 s epochs for further analysis. Epochs containing artifacts were rejected by generating a histogram of peak-to-peak amplitude for each epoch and rejecting epochs during which this value exceeded the median plus1 SD; generally, 10% of the epochs were rejected using this criterion. Artifact-free LFPs were used for all further analyses. Power spectra were calculated for each epoch by fast Fourier transform. Sample sizes (*n*) are indicated in figure legends and represent biological replicates. Sample sizes were calculated based on pilot experiments and animals were allocated randomly to different groups (opsin containing or control). Behavioral scoring and experimental assessment were performed by experimenters blind to treatment groups. Unpaired t tests were used to compare sets of data obtained from independent groups of animals. Paired t tests were used to compare behavioral data from same animals at different times. Novelty preference ratios and relative increase of gamma power compared to exploratory behaviors were analyzed using one-sample t test against the level of chance (0.5, 0; respec-

tively). All data were analyzed using Prism version 5.01 (Graphpad Software, San Diego, CA, USA). Data are presented as the mean ± SEM and statistical significance is considered at $p < 0.05$. *Peptide analysis.* The neuropeptides quantification was performed on MaxQuant software (Tyanova et al., 2016a) with the unspecific enzyme digestion setting for Uniprot rat database searching. DimethLys0 and DimethNter0 were specified as ''Light Labels''; DimethLys8 and DimethNter8 were specified as ''Heavy Labels,'' with 3 maximum labelings for each peptide. Pyroglutamylation from glutamic acid and glutamine (N-terminal), and oxidation on methionine were selected for the variable PTMs with 3 maximum modifications for each peptide. The second search was performed on only samples containing rat neuropeptides or hormone derived potential precursor form a self-made database. The neuropeptides identification was conducted on Peaks Studio Software5.3 (BSI, Waterioo, Ontario, Canada) with all raw files. The refinement and *De novo* were conducted with the same parameters: the mass tolerance of precursor ions and fragment ions with 10 ppm and 0.05 Da, respectively. No enzyme was specified for cleavage. The N termini and lysine residues was set variable modification as different dimethyl isotope labels with monoisotopic mass increment of light (28.0313 Da) and heavy (36.0756 Da), respectively. Others variable modifications setting are consistent with MaxQuant.

The identification was based on rat database downloaded from Uniprot (January, 2017). The quantification was performed on target neuropeptides database that contains the neuropeptides and hormone related precursors only. The target database was integrated from different sources: Neuropeptide Database (www.neuropeptides.nl), Sweden peptide Database (www.swepep.org), and other hormone related peptides (https://uniprot.org/uniprot/) reported in Nature Communication (Secher et al., 2016). An FDR of 1% was specified as the cutoff for false discovery rate for peptide identification and quantification. Manual inspection was conducted to improve the neuropeptide identification accuracy as previous described (Petruzziello et al., 2013). Neuropeptides that were identified by both programs were collected to perform quantification with the Perseus program (Tyanova et al., 2016b). Statistical analysis was conducted on significant A with p value (FDR < 0.05) after log2 calculation. At least two valid values and the same alteration direction neuropeptides were collected. The amino acids sequence motifs were created by pLogo program (https://plogo.uconn.edu/) (O'Shea et al., 2013).